General Disclaimer

One or more of the Following Statements may affect this Document

- This document has been reproduced from the best copy furnished by the organizational source. It is being released in the interest of making available as much information as possible.

- This document may contain data, which exceeds the sheet parameters. It was furnished in this condition by the organizational source and is the best copy available.

- This document may contain tone-on-tone or color graphs, charts and/or pictures, which have been reproduced in black and white.

- This document is paginated as submitted by the original source.

- Portions of this document are not fully legible due to the historical nature of some of the material. However, it is the best reproduction available from the original submission.

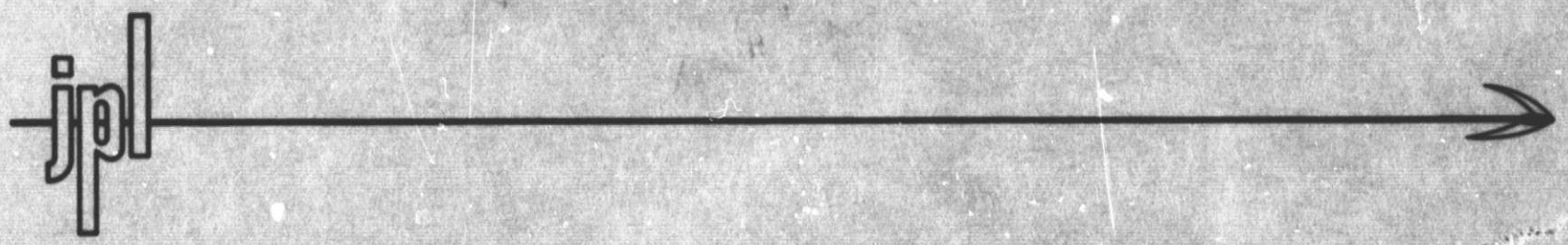

JET PROPULSION LABORATORY
CALIFORNIA INSTITUTE OF TECHNOLOGY
PASADENA, CALIFORNIA

760-44

CRATER DEFLECTION STUDIES

March 20, 1970

Ritchie B. Coryell
and
Larry Durr

Approved by:

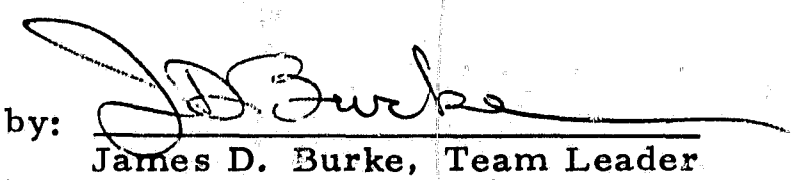

James D. Burke, Team Leader
Advanced Lunar Studies

JET PROPULSION LABORATORY
CALIFORNIA INSTITUTE OF TECHNOLOGY
PASADENA, CALIFORNIA

ACKNOWLEDGEMENT

The authors wish to acknowledge the technical assistance of D. Page and J. Pinneo in the model crater tests and R. A. Mills, J. Crossen, A. Dahl, W. Roeder, J. Running, B. G. Tinnin, I. L. Wiser, and G. Ulrich, all of the U. S. Geological Survey, in full-scale crater tests near Flagstaff, Arizona.

TABLE OF CONTENTS

SECTION I

INTRODUCTION

The path traced by a wheeled vehicle on the lunar surface is influenced not only by its steering parameters but also by the terrain and other vehicle parameters. The purpose of the experiments reported in this document was to gain a first-order understanding of the deflection to which a vehicle, with wheels locked in a dead-ahead position as it traversed a crater, would be subjected.

These experiments involved a statistical test using a model vehicle that traversed craters constructed in sand. No attempt was made either to scale the vehicle to experimental size or to simulate the lunar environment. Details of the model vehicle's track in the crater and data on wheel slip, power, and other performance parameters were not measured in these experiments. Rather, the objective was an inexpensive, large statistical sample of the crater deflection of a model vehicle.

The crater deflection problem is somewhat similar to the classical scattering problem in which a particle approaching a scattering center is deflected. The deflection angle is a function of certain particle parameters, (e. g., momentum), parameters of the scattering body, (e. g., field strength), and the impact parameter, which is the miss distance.

For crater deflection, the deflection angle δ is not uniquely determined by the known parameters of the vehicle and crater, and the offset distance a, the corollary of the impact parameter. This may be because not all relevant conditions of a test run can be known or precisely measured and reproduced. Some attempts at a deterministic model of soil mechanics parameters and wheel/soil interactions may lead successfully to a deterministic crater deflection model. Results from these stochastic experiments provide hints as to some properties of such a model and data for calculation of some limited performance characteristics of a wheeled vehicle on the cratered surface of the moon.

This document reports the experimental apparatus and procedures, a statistical summary of the experimental data, and salient features of the results. A proposed stochastic model for crater deflection and computer simulations of passage through a crater field that utilize this model are expected to be reported in subsequent documents.

SECTION II

EXPERIMENTAL APPARATUS

A. MODEL APPARATUS

The model apparatus consisted of two major components: (1) the model vehicle and its power supply, and (2) the crater-shaping tool and sandbox. Detailed views of the apparatus are shown in Figures 1 through 5. In addition, smaller wheels, ballast, and a six-wheel model vehicle were used in special test runs.

1. Model Vehicle and Power Supply

An off-the-shelf, four-wheel drive, battery-powered toy, Marx model No. 6321, provided the basic gear train, electric motor, and chassis for the model vehicle (Figure 1). Several modifications necessary to satisfy the specific requirements of the experiment were made.

The body was discarded to reduce vehicle weight and to allow for the clearance of oversized wheels. Large wheels (Figure 2) were added for two reasons: (1) to reduce the footprint pressure and thereby improve the capability of the vehicle to traverse loose soil, and (2) to increase the speed of the vehicle. Two banana jacks were mounted on the chassis and two electrical wires were run from the model to an external 3- or 6-vdc power supply. Care was taken to avoid applying steering torques through the wires. This substitution for batteries lightened the model weight and provided a more balanced distribution of weight between front and rear axles (45:55%, respectively). The model in its modified form and ready for use in the experiment had a gross weight of 342 g, a wheel-base of 4 3/8 in. (Figure 3), a track width of 4 in. outside to outside, and a wheel diameter of 4 3/16 in. Rated ground speeds were 0.5 and 0.8 ft/sec with 3 and 6 v, respectively, applied to the motor.

2. Crater-Shaping Tool and Sandbox

The crater-shaping tool (Figure 4) was a device that rotated a template shaped to the cross-section of a crater of interest. Sand was then back-filled to the outside dimensions of the rotating template. The crater-shaping tool was mounted to a pivoting structure, attached to the sandbox, that could rotate away from the completed crater to allow passage of the model vehicle through the

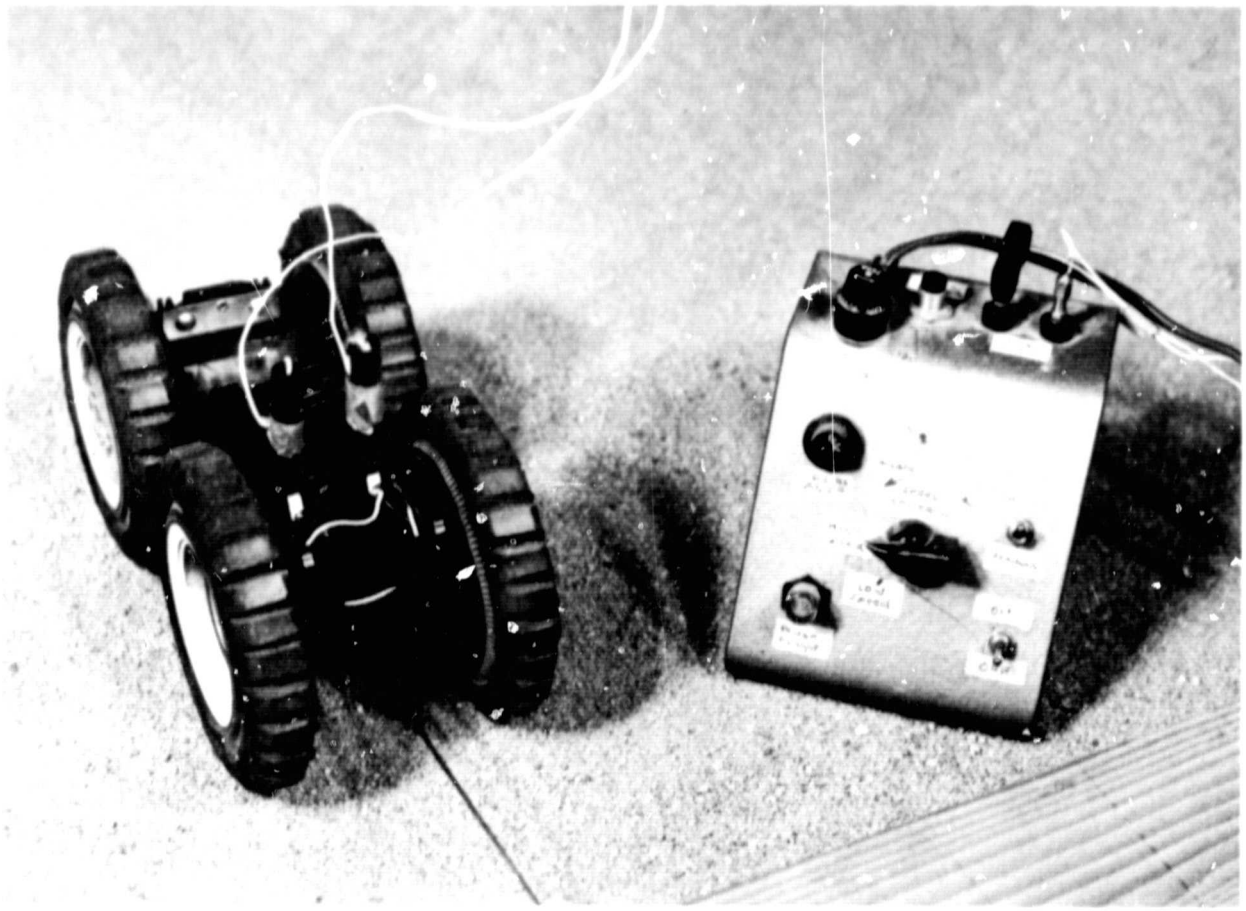

Figure 1. Model Vehicle and Power Supply

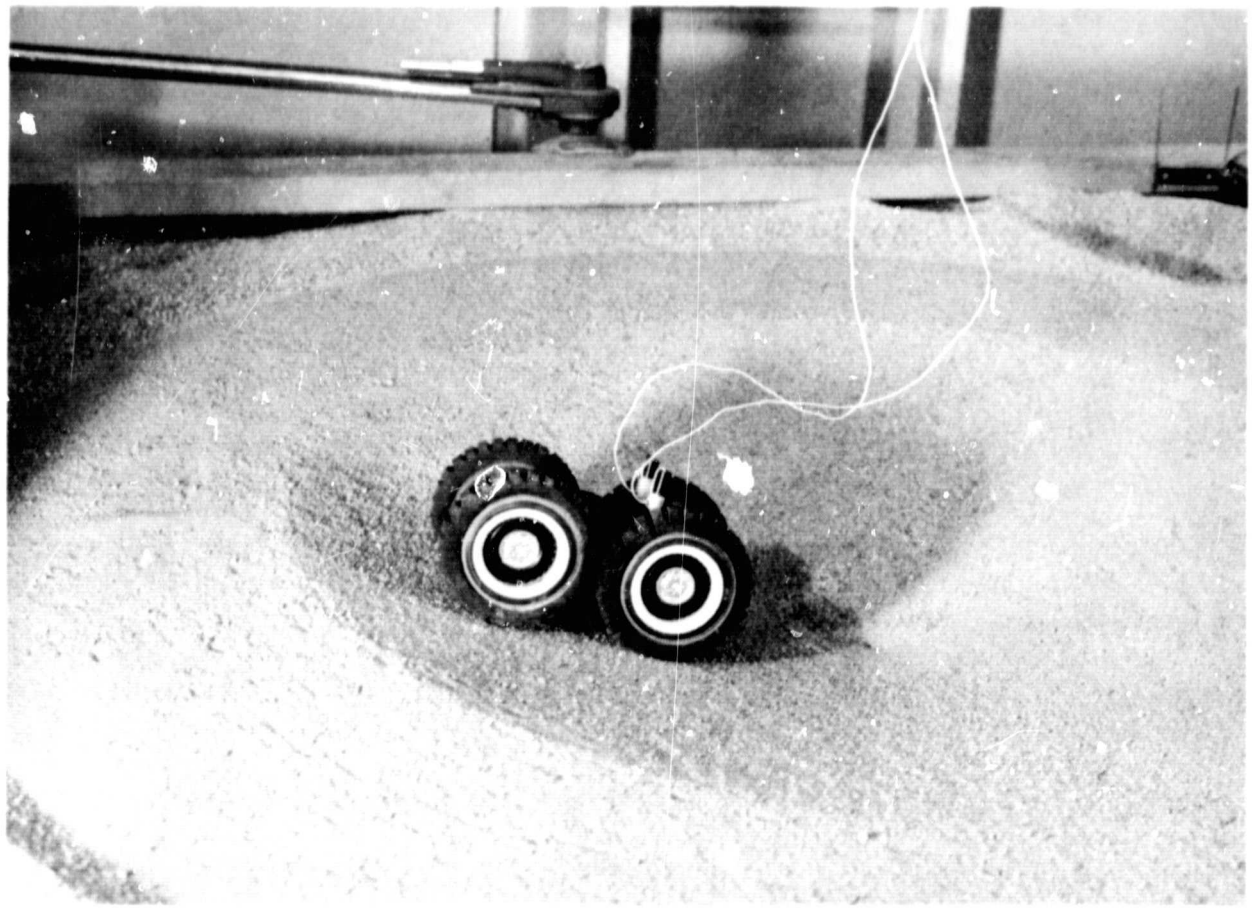

Figure 2. View of Model Vehicle Showing Larger Wheels

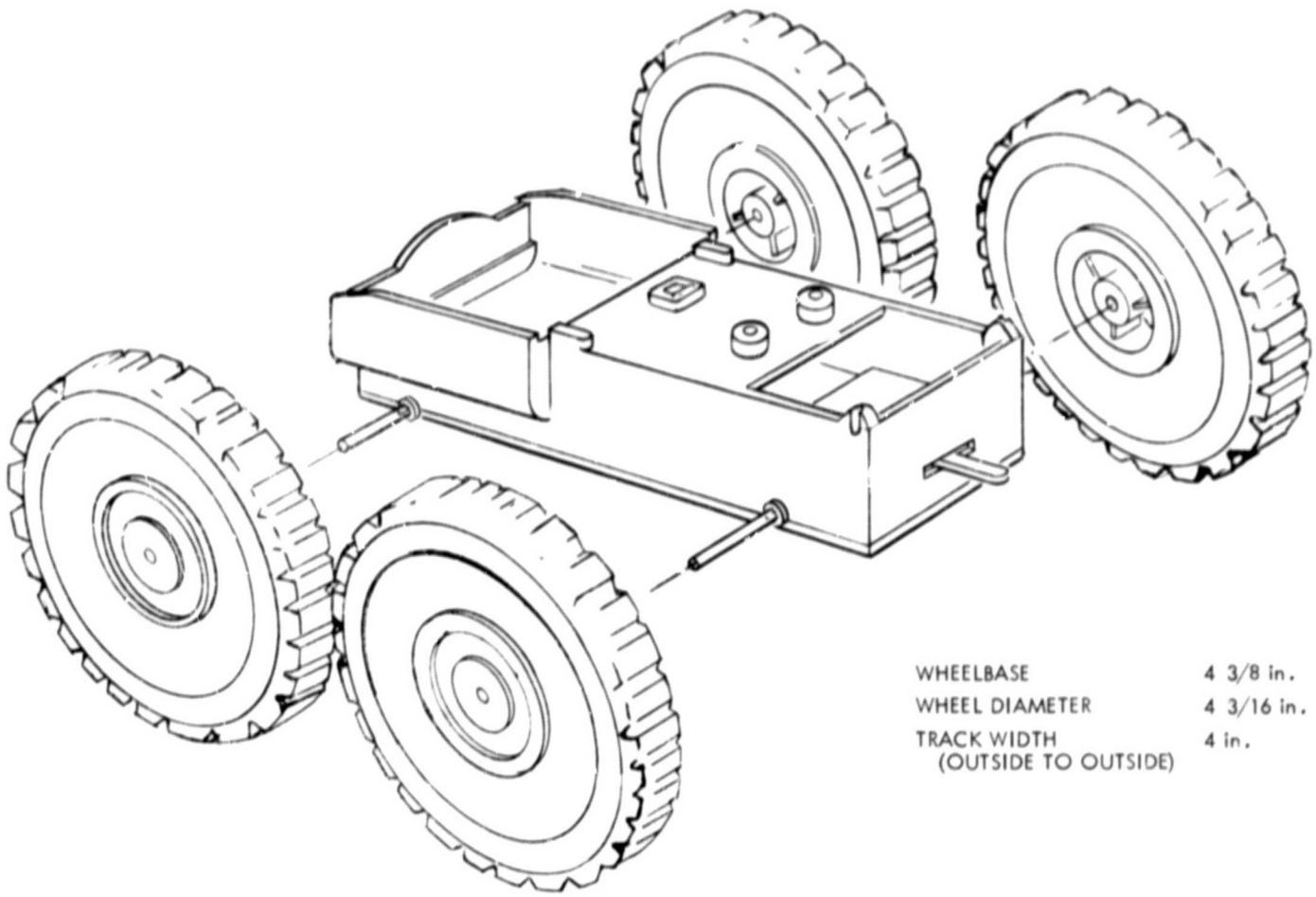

Figure 3. Three-Quarter Exploded View of Model Vehicle with Dimensions

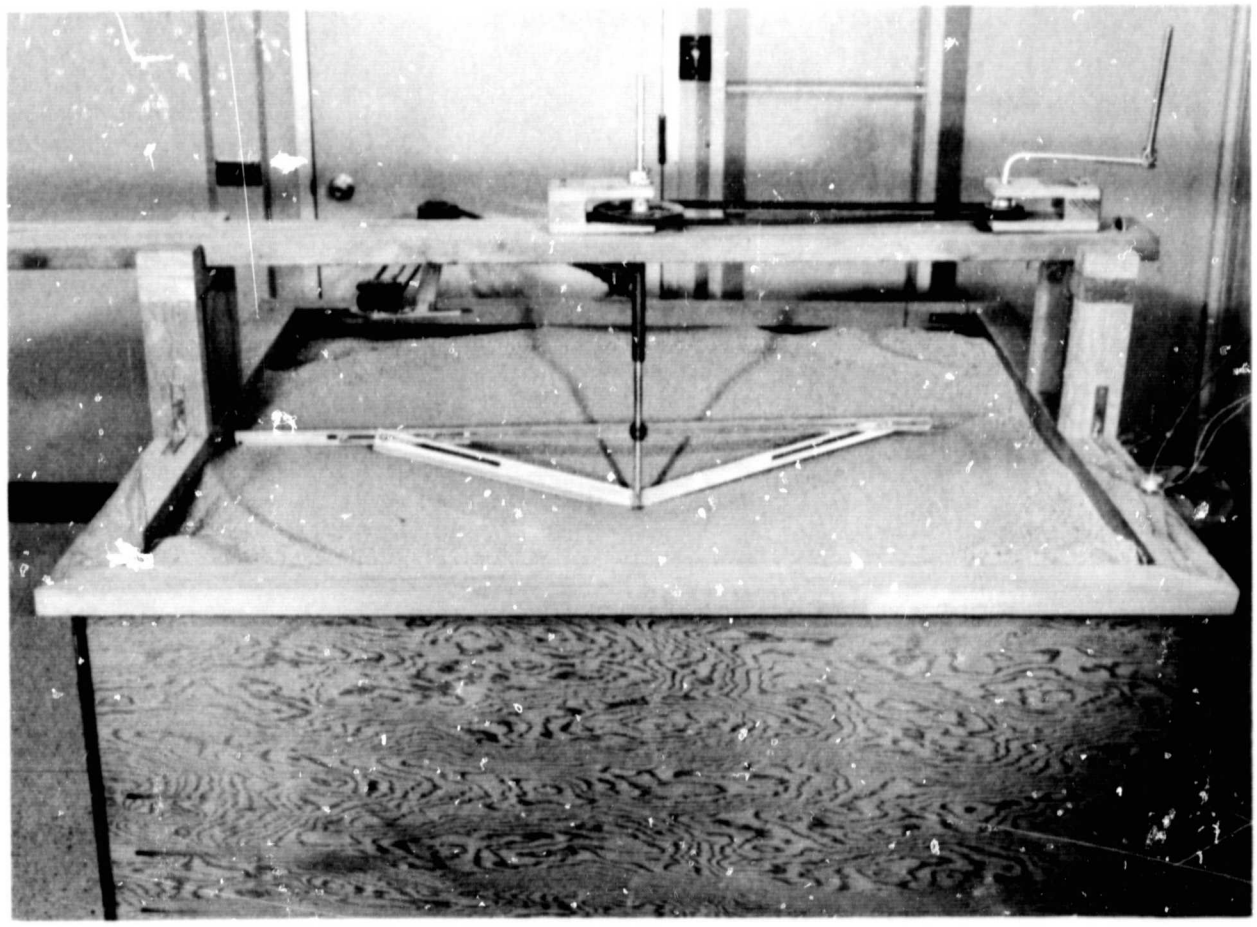

Figure 4. Crater-Shaping Tool and Sandbox with Tool in Place

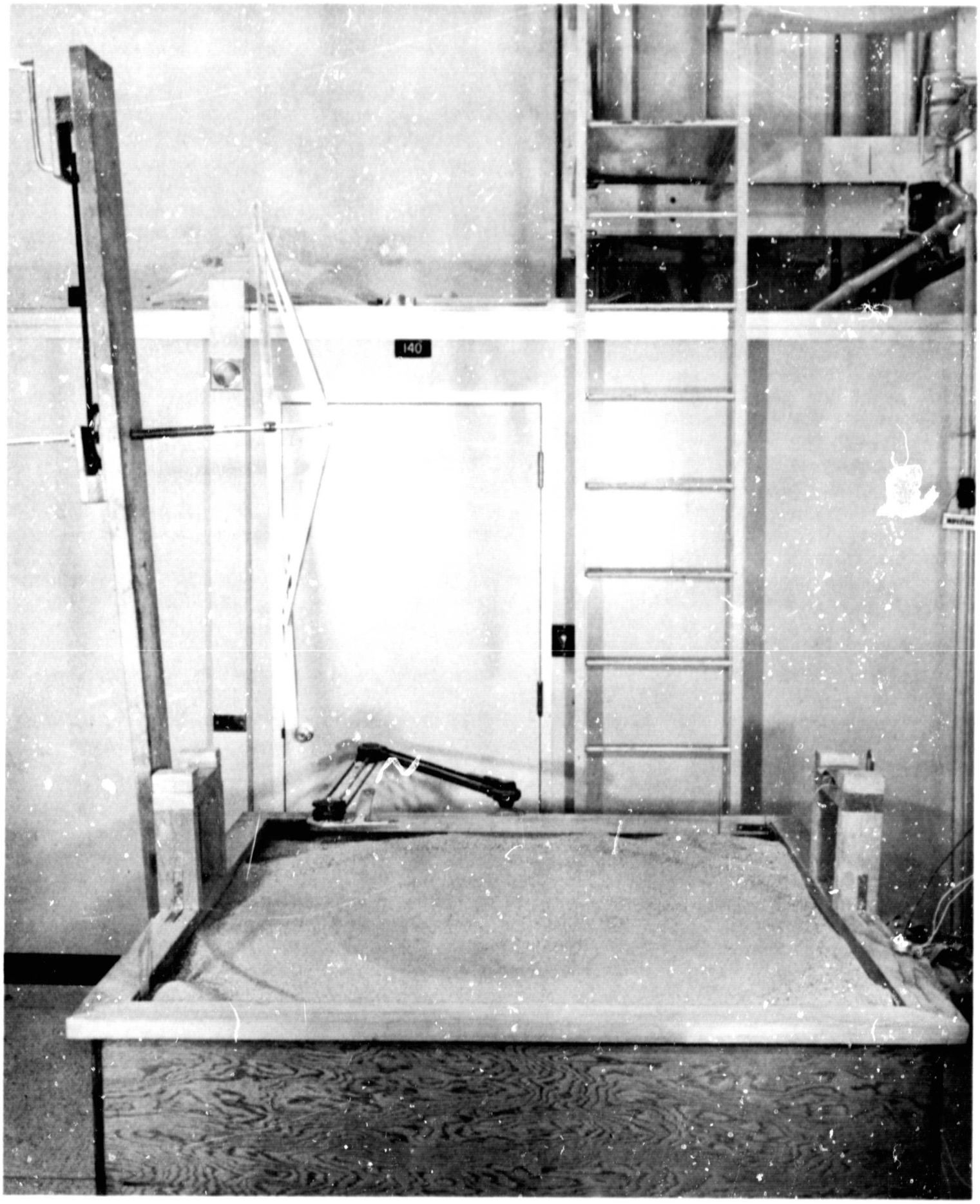

Figure 5. Crater-Shaping Tool and Sandbox with Tool Removed

crater (Figure 5). On a vehicle transit, the template could be pivoted back to the same position to remove vehicle tracks or deformations of the crater walls so that the model could traverse the crater again.

3. Other Model Apparatus

The smaller wheel was 2 3/4 in. in diameter. Ballast weighing 110 g increased vehicle weight by 32%. The six-wheel vehicle included a four-wheel truck and a two-wheel trailer. The truck and the trailer were independently powered. The speed of the truck was regulated to be slightly greater than that of the trailer. The truck was identical to the previously described four-wheel vehicle with wheelbase of 4 3/8 in., and the wheelbase of the trailer, from the rear axle of the track, was 4 3/4 in. Both had wheel diameters of 2 29/32 in., and a track width of 3 in. center-to-center. Smaller wheels were used rather than the 4 3/16 in. -diameter wheels to avoid interference between truck and trailer in tight turning situations. The trailer was attached to the truck with a universal joint, which permitted 360 deg rotation in roll and 90 deg rotation in pitch and yaw.

B. FULL-SCALE VEHICLE AND CRATERS

Crater deflection tests were made with the four-wheel Explorer vehicle (Figure 6) in a simulated lunar crater field near Flagstaff, Ariz. The vehicle and the craters, in a cinder field near the foot of Sunset volcanic crater, were made and maintained by the Astrogeology Branch of the U. S. Geological Survey (USGS).

The Explorer has a 10-ft wheel base and weighs approximately 2 tons; the weight is distributed approximately 60% on the front axle and 40% on the rear. Its center-to-center track width is 75 in.

Although a large number of smaller craters were available at the site, two were selected for the test, one 47 ft in diameter and the other 57 ft in diameter. The intent was to approximate the ratios of crater diameter to vehicle wheelbase that were used in the model tests. For the model tests, these ratios were 5.5:1, 6.9:1, and 8.2:1. The 57-ft crater had a 5.7:1 diameter-to-wheelbase ratio, approximating the ratio for the model 24-in. crater.

Figure 6. Four-Wheel Explorer Vehicle

Although the diameter-to-wheelbase ratio for the 47-ft crater fell below the range for model tests, it was used for test runs to gain experience and to test the Explorer's capability for passage through large craters. Test runs on an 80-ft-diameter crater were not attempted because its long and steep walls were considered hazardous to vehicle and driver. Even if the vehicle were not to turn over, it was thought that it would sink deeply into the soft soil of the slope and fail to climb out on its own power.

The smaller crater used has a depth-to-diameter ratio of 1:4.3, and the 57-ft crater has a 1:4.1 depth-to-diameter ratio. They are nearly conical in shape; slumping is responsible for slightly steeper slopes at the tops of a crater wall than at the bottom. They have slight exterior rims but probably not enough to make a difference in the deflection measurements. The 57-ft crater is on a slight slope at right angles to the direction of the test runs, so that the rim at its highest point is 1.67 ft higher than on the opposite side.

SECTION III

EXPERIMENTAL PROCEDURES

A. MODEL TEST PROCEDURE

The following is the step-by-step procedure used to collect the data in this experiment.

1. Adjust crater shaping tool to proper dimensions and shape the crater (Figure 4).
2. Raise and retract crater-shaping tool (Figure 5).
3. Adjust drafting machine to zero deflection by aligning it with front edge of sandbox.
4. Using a large drafting triangle, place the vehicle alignment guide perpendicular to the front side of sandbox at the desired offset distance (Figure 7).
5. Place vehicle astride the alignment guide, apply electrical current to the vehicle, and allow it to traverse the crater from rim-to-rim.
6. Place alignment guide along the exit path of the vehicle, and using drafting machine, measure the exit angle of the vehicle (Figure 8).
7. Record the measured deflection angle δ, crater diameter D, and offset distance a in a log (Figure 9).
8. Repeat steps 1 through 7.

B. FULL-SCALE TEST PROCEDURE

With the following exceptions, the steps followed in the experiment with the Explorer near Flagstaff, Ariz. were identical with those of the model test procedure.

(1) For a given offset distance a, only one trial run was made.

(2) Some trial runs had to be omitted for fear of overturning or damaging the vehicle.

(3) Starting positions were established by flags laid out by USGS surveyors.

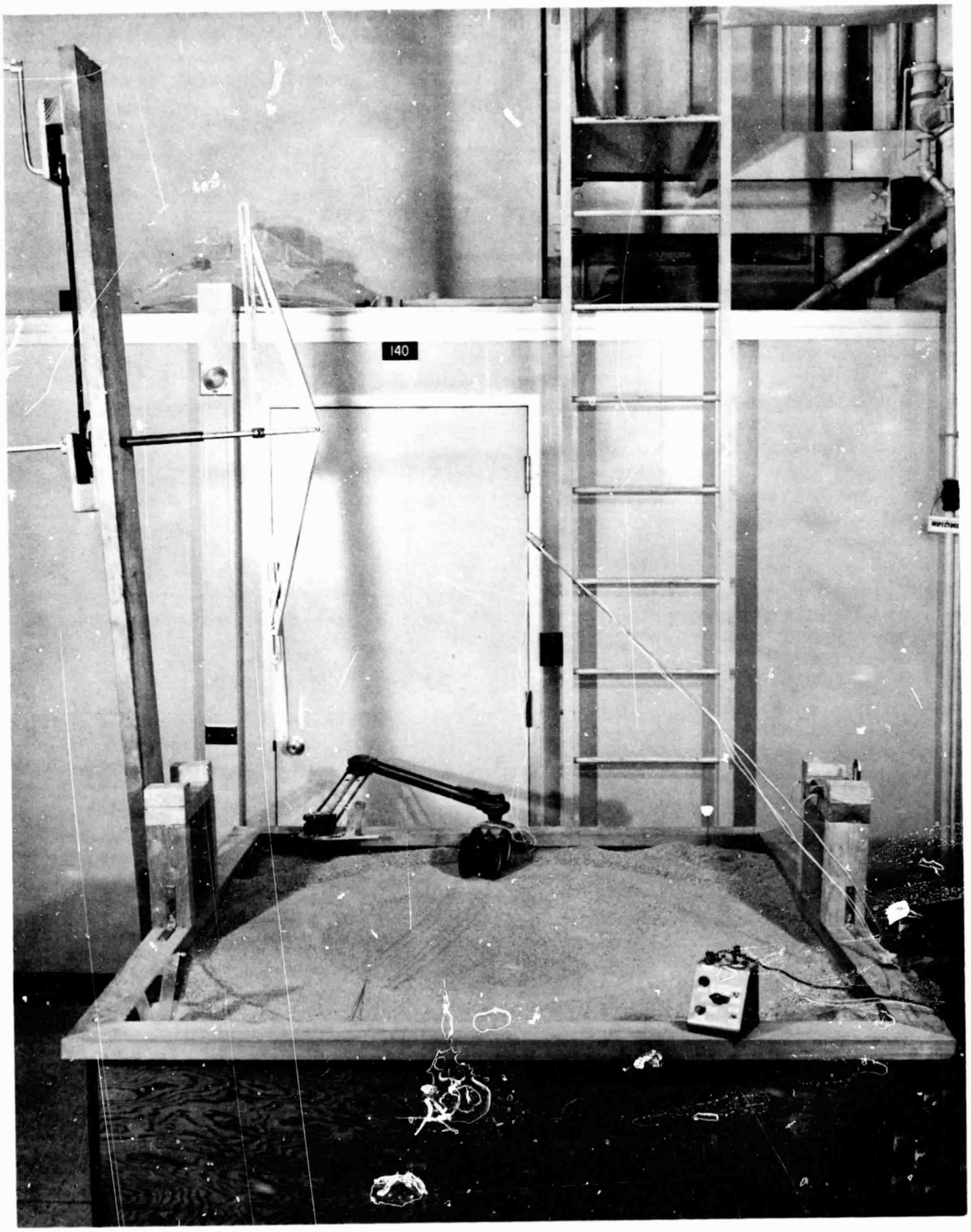

Figure 7. Model Vehicle Mounted on Alignment Guide

Figure 8. Procedure for Measuring Exit Angle of Vehicle

TRIAL	OFFSET DISTANCE ±a, in												
	-12	-10	-8	-6	-4	-2	0	+2	+4	+6	+8	+10	+12
1	-4	-4	-6	-1	-5	0	-2	-1	+3	+5	+5	+2	+2
2	0	-3	-6	-4	-4	-2	-1	+1	+1	+1	+3	-1	+3
3	-3	-4	-5	-2	-2	-2	+1	-1	+4	+4	+1	0	+2
4	-1	-3	-5	-6	-4	+2	+1	+1	+3	+3	+5	+3	+2
5	-1	-6	-3	-4	-2	+2	+2	+2	-1	0	+2	+1	+1
6	-2	-5	-5	-5	+1	+2	-1	+1	+4	+4	+4	+2	0
7	-2	-4	-5	-3	-3	+1	+3	-2	+1	+3	+4	+3	-1
8	-1	-4	-3	-3	-2	+1	0	0	+2	+3	+4	+2	0
9	-1	-3	-4	0	-1	+2	0	+1	+2	+4	0	+6	0
10	-2	-2	-4	-2	0	+1	+1	+2	+1	+4	-1	+3	-2

24-in. DIAMETER

d = 2.4 in.

d/D = 1:10

δ IN DEGREES

Figure 9. Sample of Data as Recorded in Log Book

(4) Deflection angles were measured by recording before and after a trial run the bearing of the Explorer's on-board gyrocompass.

(5) Crater shaping was confined to leveling furrows on crater walls with a rake after trial runs.

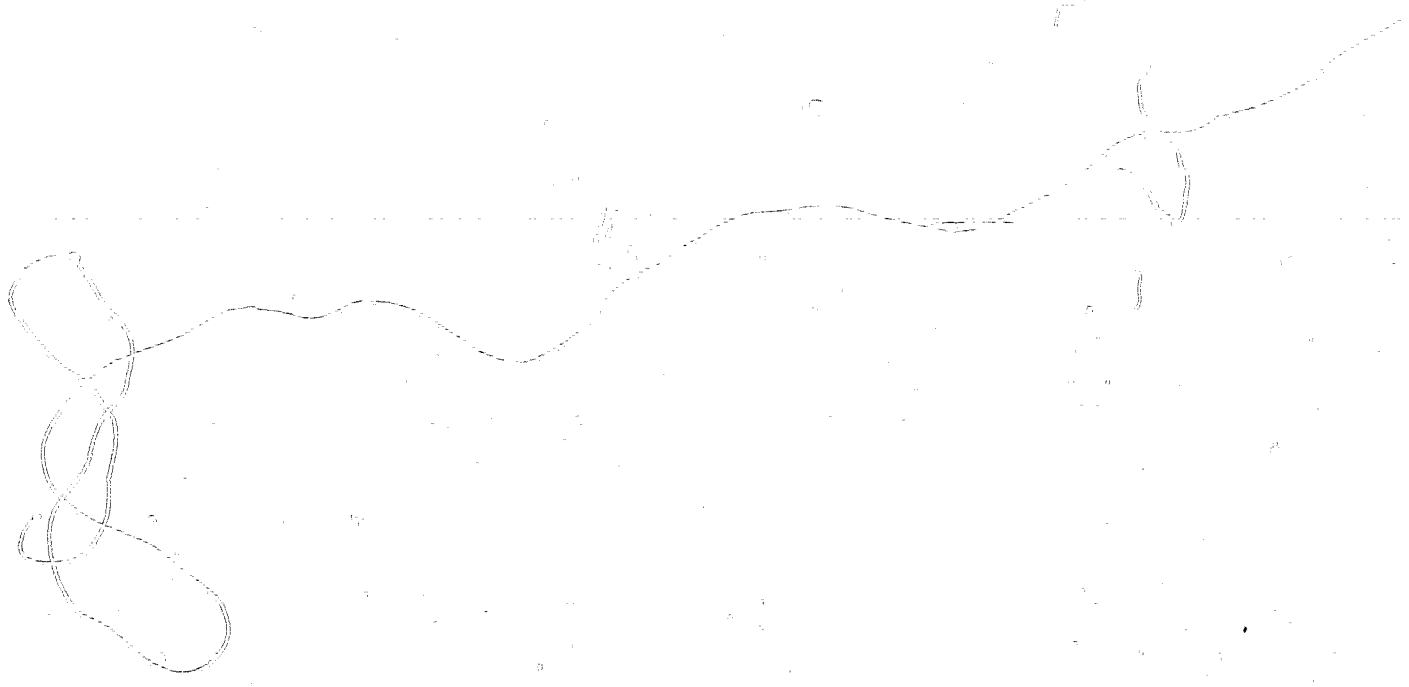

SECTION IV

TEST RESULTS

The model test data are presented in three categories:

(1) Conical craters for a range of diameters D and depth-to-diameter ratios d/D are shown in Figures 10 through 16.

(2) Craters of non-conical shapes are shown in Figure 17.

(3) Variations in the vehicle's configuration and/or physical parameters are shown in Figures 18 through 20.

The sample mean $\bar{\delta}$ plus and minus one standard deviation 1σ are plotted for each offset distance a from the center line of a crater.

Curved lines in Figures 10 through 20 connect the sample means for a particular series of test runs. These curves are only an aid in analyzing the data and are not proposed as theoretical functions, $\bar{\delta}(a)$.

Measurements made with the Explorer vehicle at the USGS test site near Flagstaff, Ariz. are shown in Figures 21 and 22.

Certain qualitative observations of the results can be made. Because conical craters were most easily constructed, more complete information was obtained for these craters.

A. SYMMETRY

There is a recognizable symmetry of the data about the $\delta = 0$ and $a = 0$ axes. That is, a left-handed offset produces deflections to the right symmetrical with the left deflections of right-handed offsets.

A measure of the symmetry is the root-mean-square (rms) of differences between corresponding sample means after rotation about the axes of symmetry, or

$$RMS_1 = \sqrt{\sum_a \left\{ \bar{\delta}(a) - \left[-\bar{\delta}(-a) \right] \right\}} = \sqrt{\sum_a \left[\bar{\delta}(a) + \bar{\delta}(-a) \right]}$$

This symmetry index as computed for each of the 36-in. -diameter conical craters is shown in Table 1.

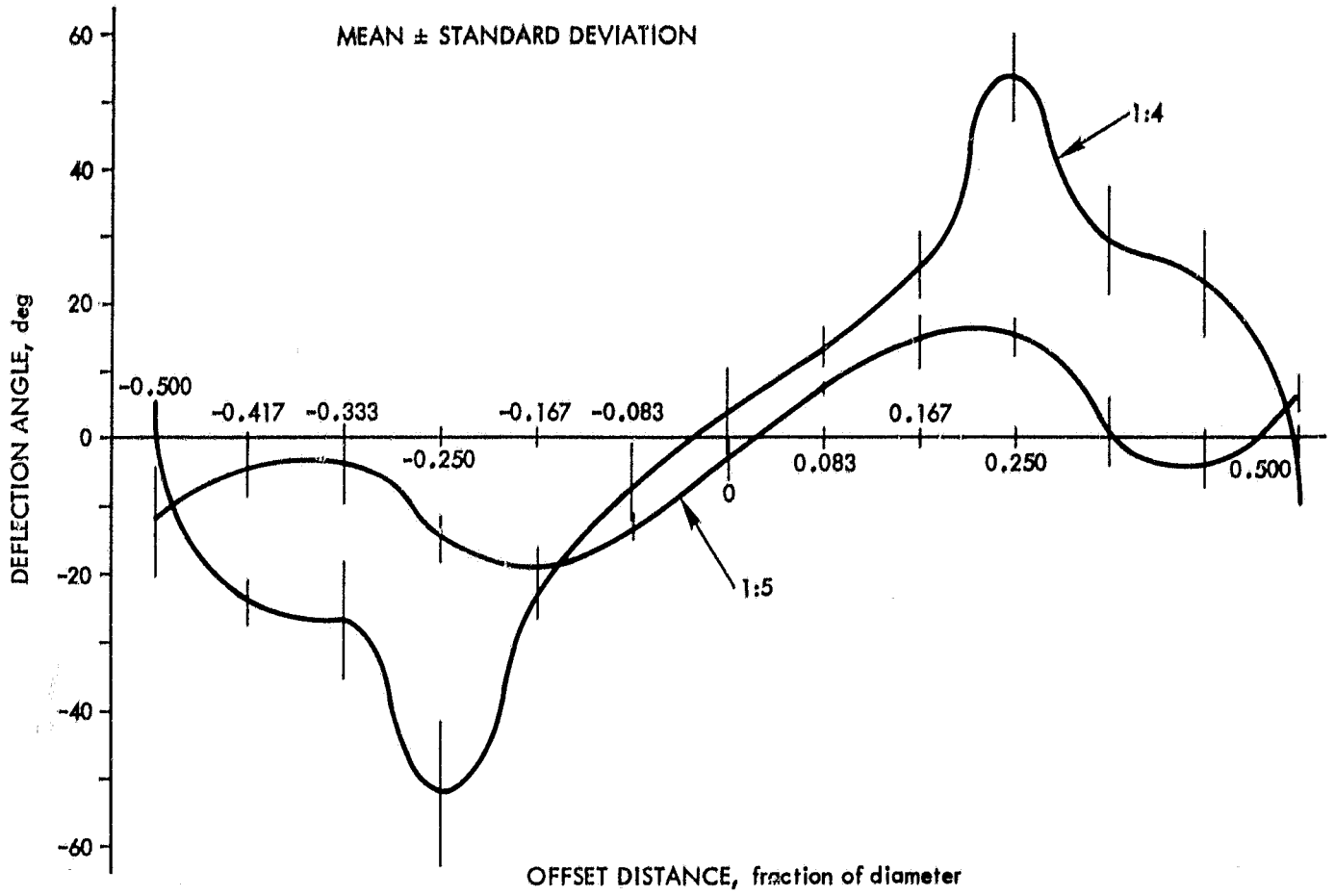

Figure 10. Crater Deflection Data, 36-in. -Diameter, d/D Ratios 1:4 to 1:5

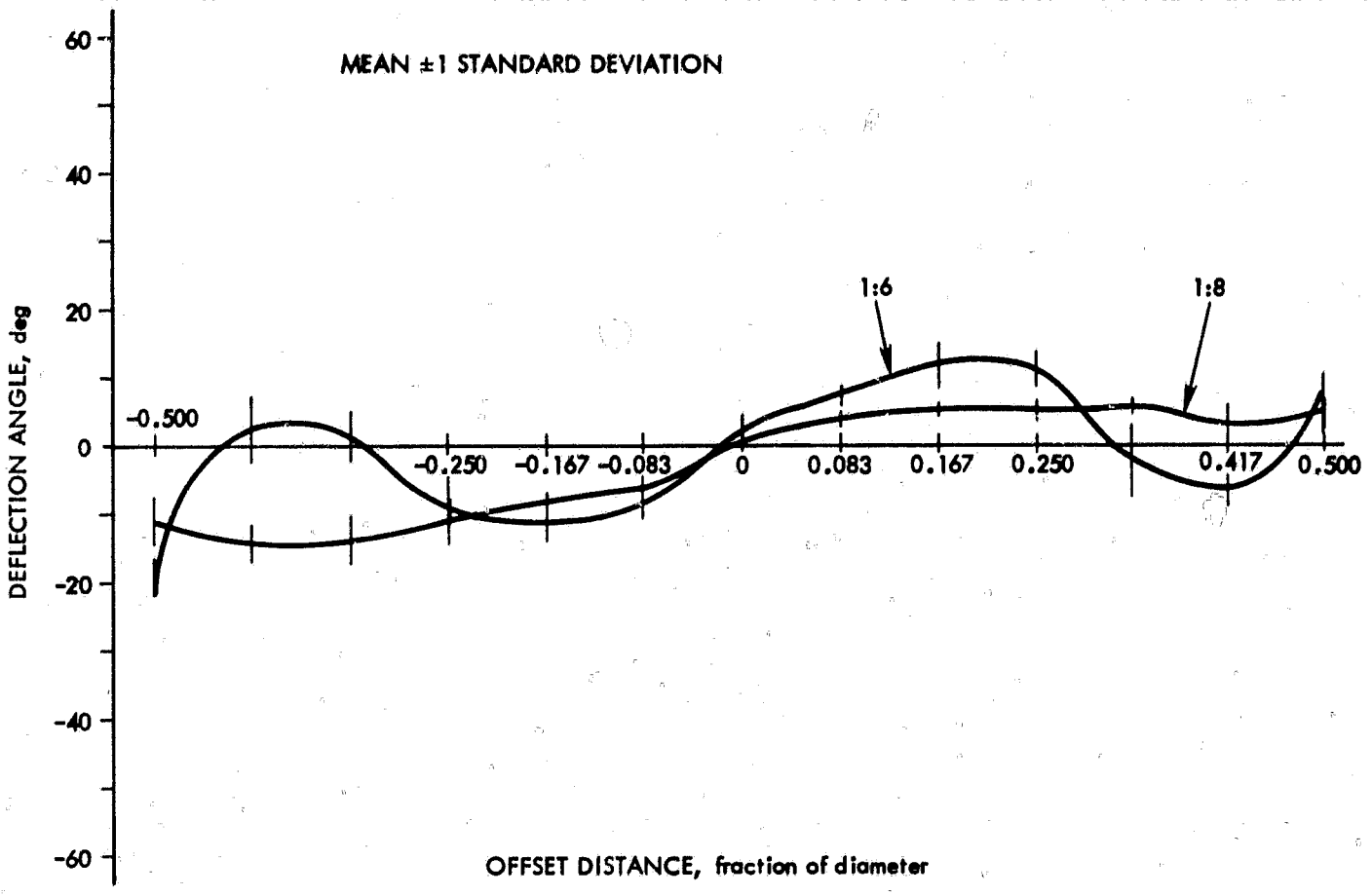

Figure 11. Crater Deflection Data, 36-in. Diameter, d/D Ratios 1:6 to 1:8

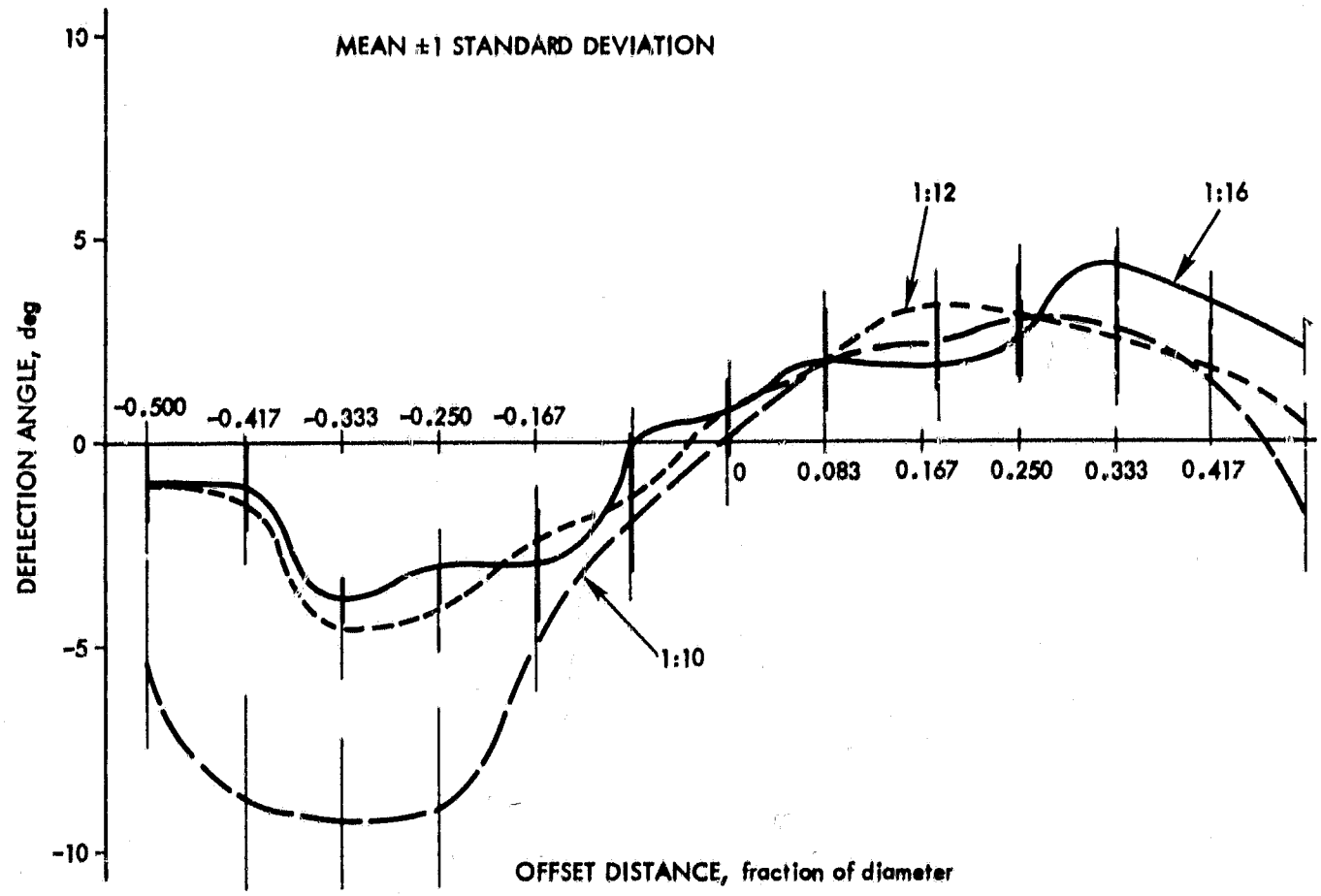

Figure 12. Crater Deflection Data, 36-in. Diameter, d/D Ratios 1:10 to 1:16

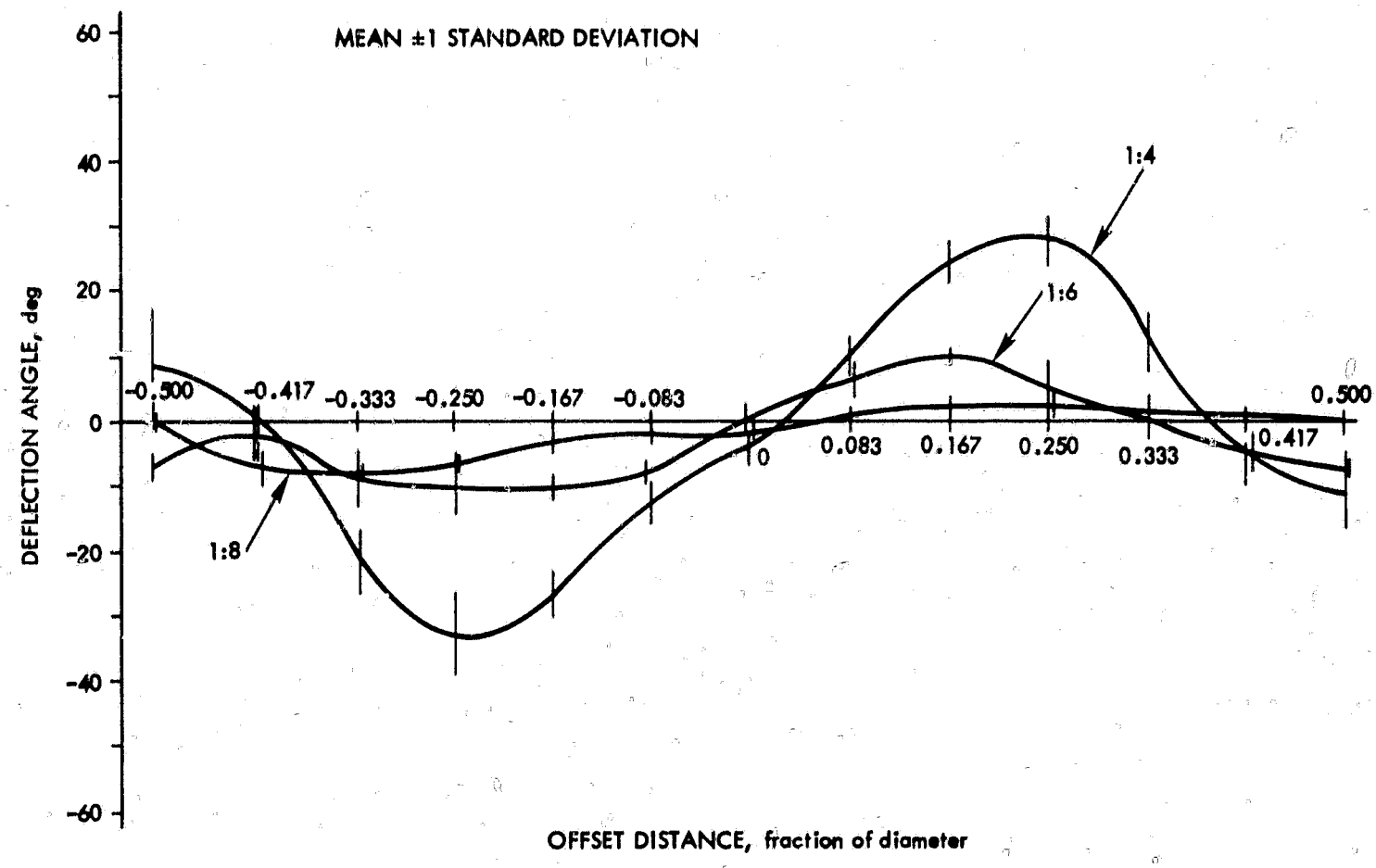

Figure 13. Crater Deflection Data, 30-in. Diameter, d/D Ratios 1:4 to 1:8

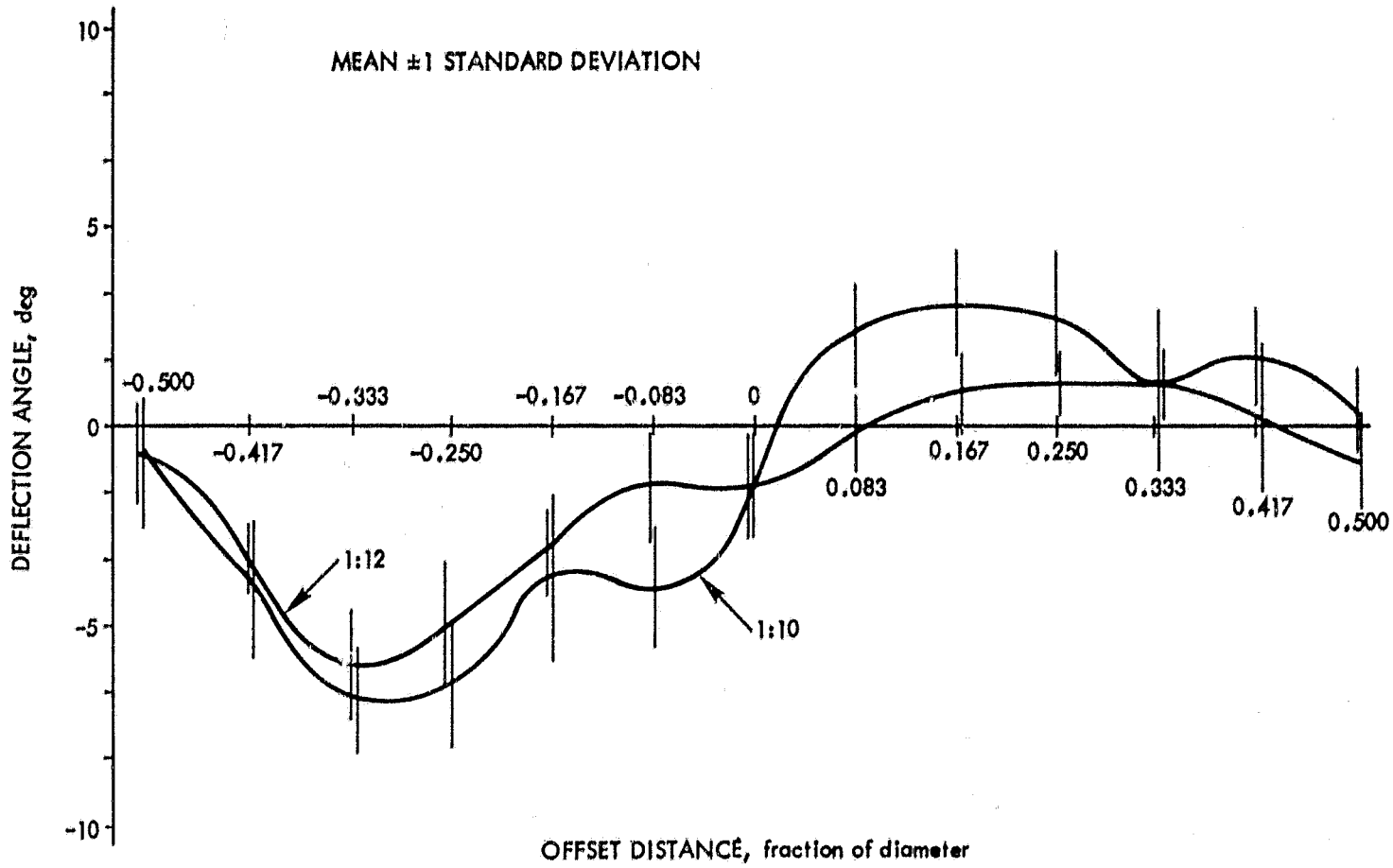

Figure 14. Crater Deflection Data, 30-in. Diameter, d/D Ratios 1:10 to 1:12

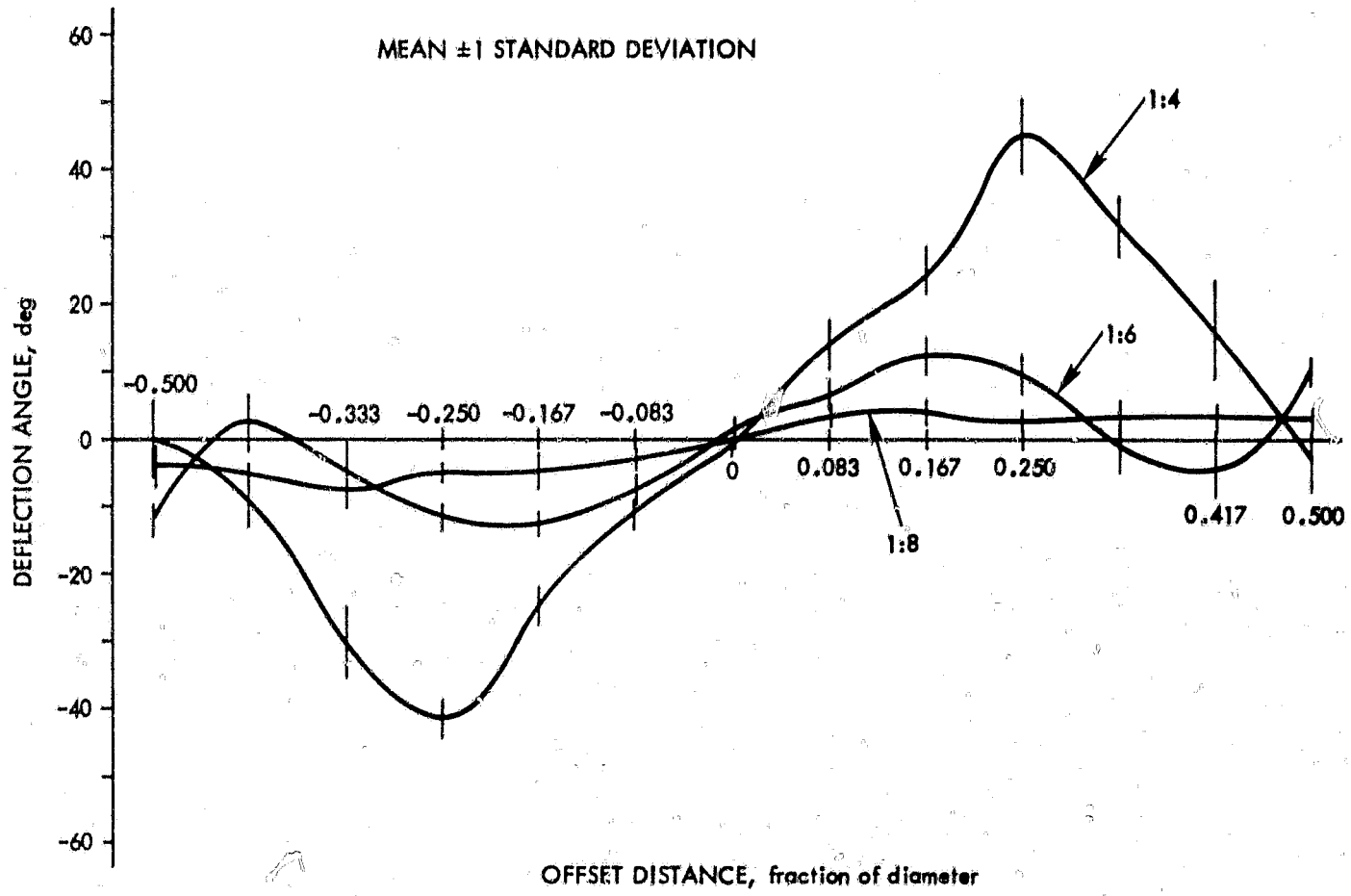

Figure 15. Crater Deflection Data, 24-in Diameter, d/D Ratios 1:4 to 1:8

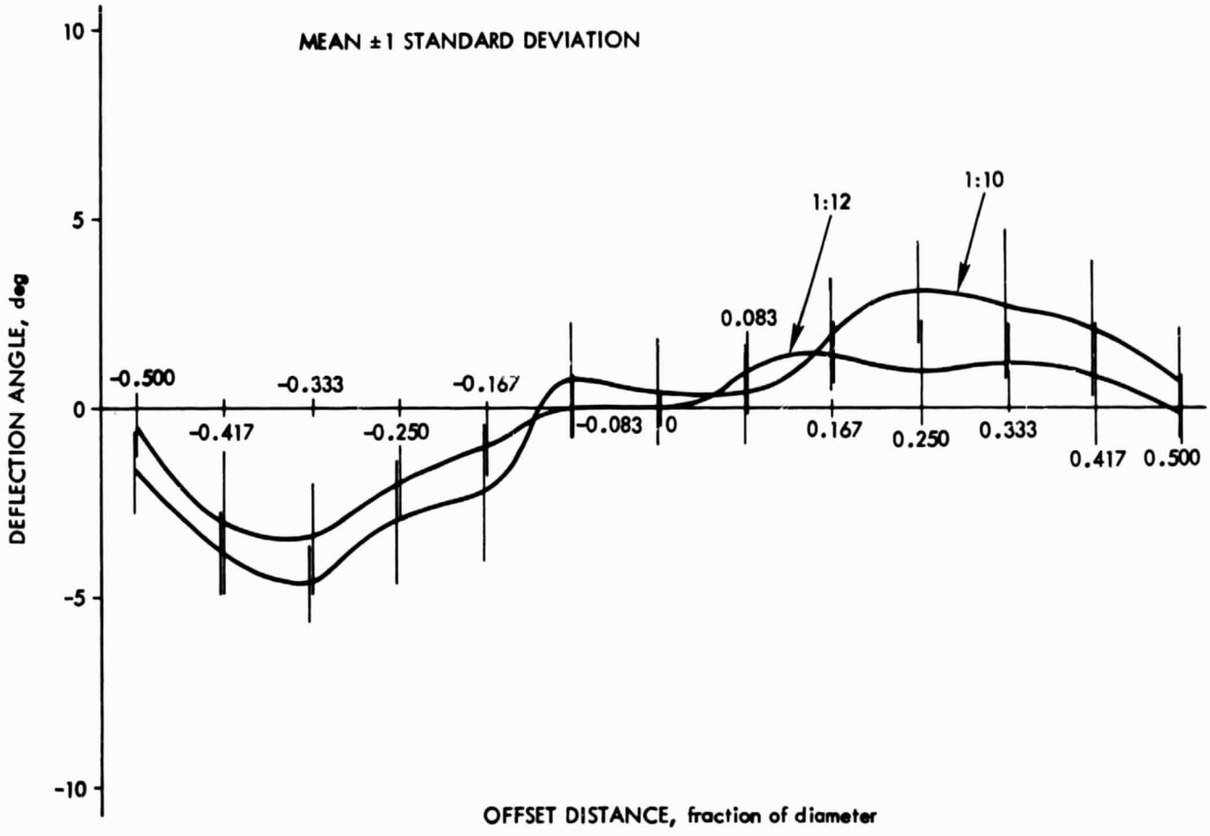

Figure 16. Crater Deflection Data, 24-in. Diameter, d/D Ratios 1:10 to 1:12

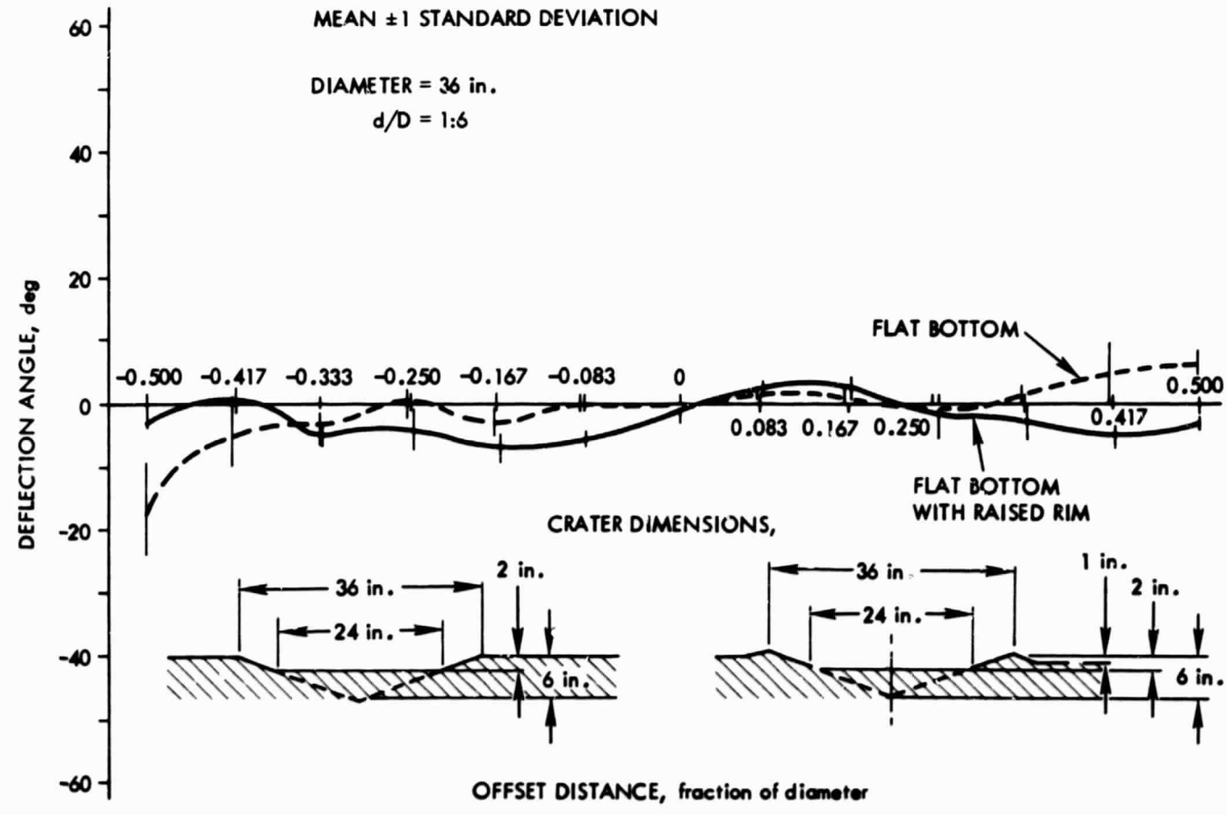

Figure 17. Crater Deflection Data, Nonconical Shapes

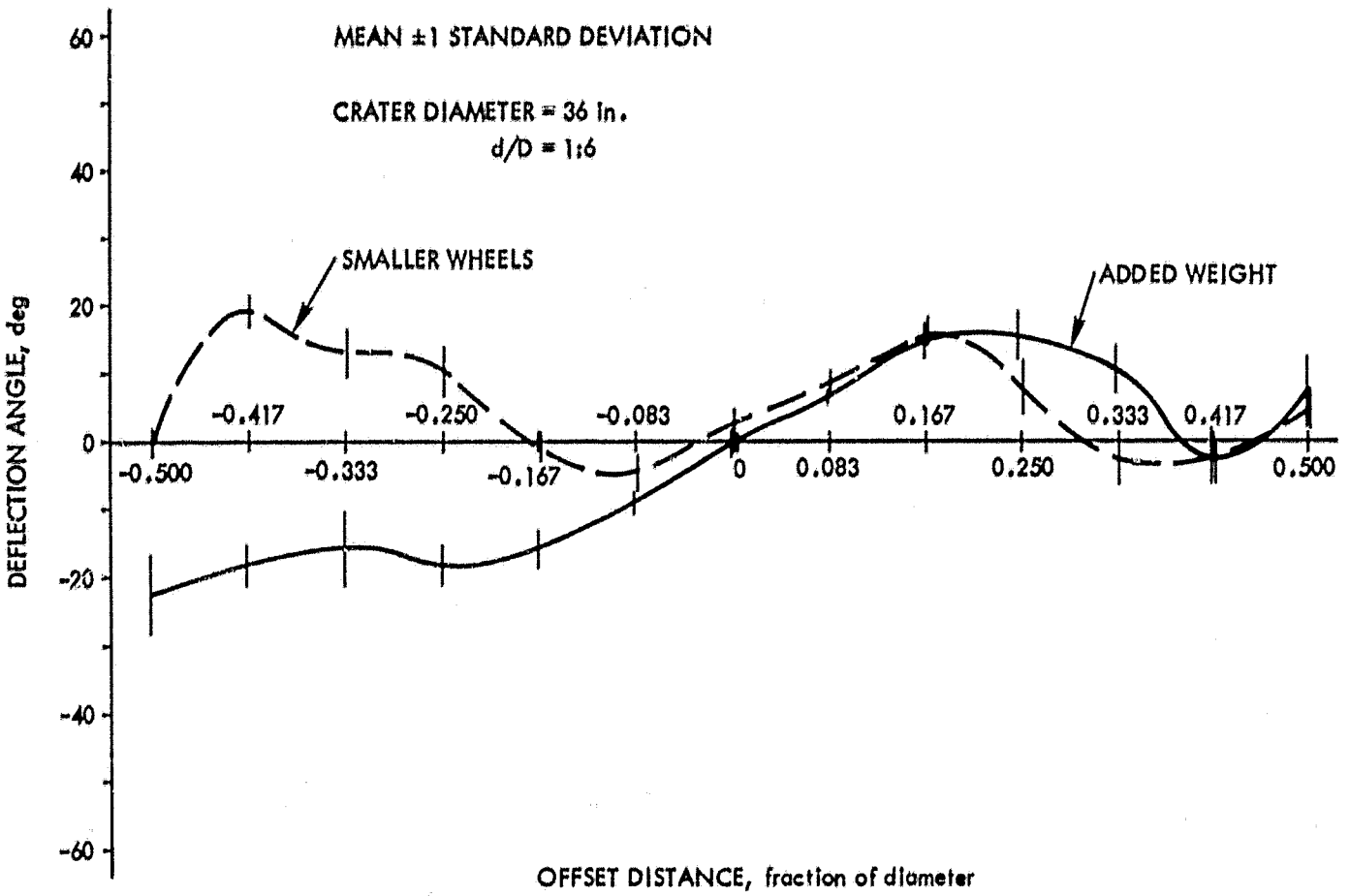

Figure 18. Effect of Smaller Wheels and Added Weight on Crater Deflection Data

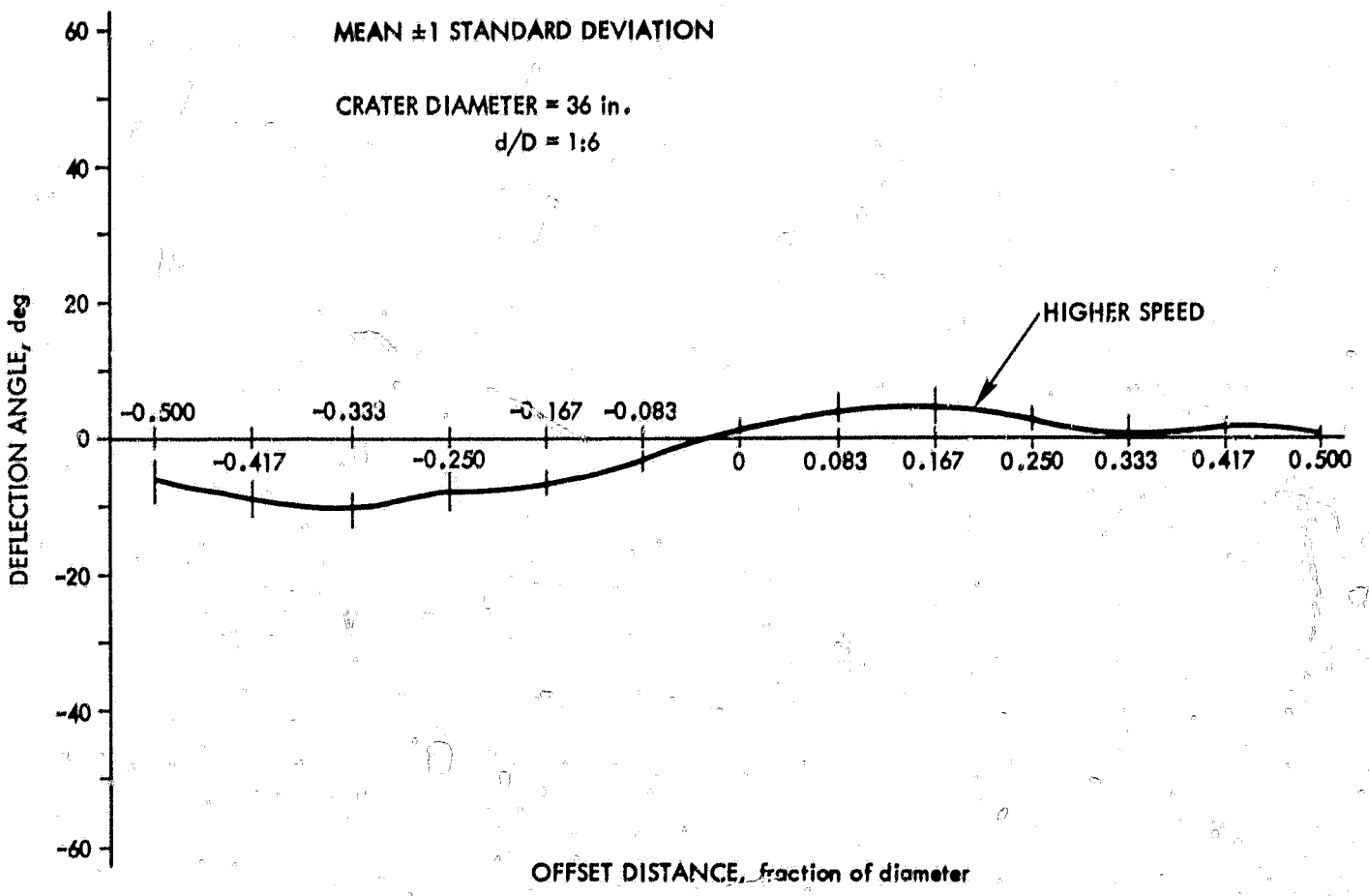

Figure 19. Effect of Higher Vehicle Speed on Crater Deflection Data

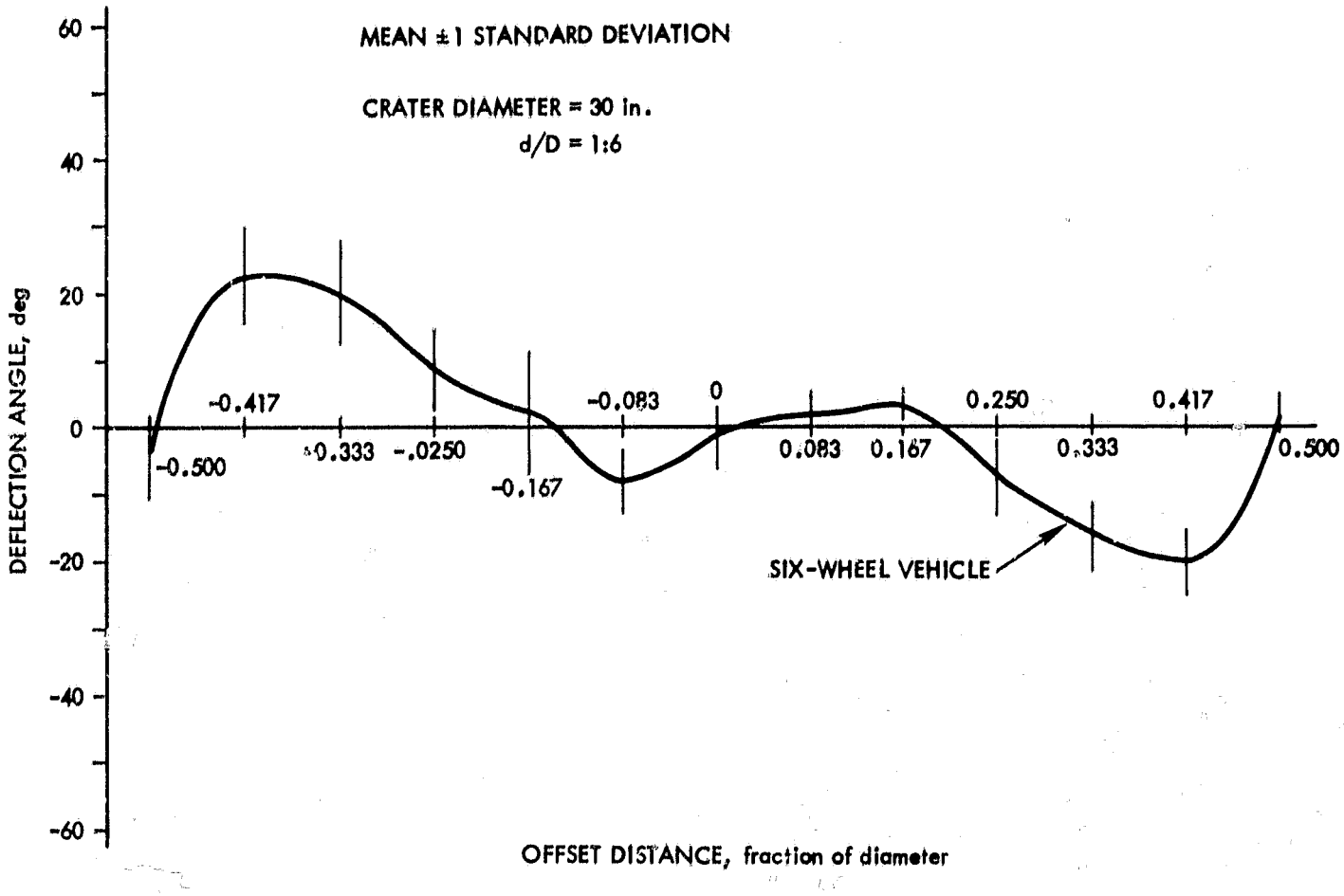

Figure 20. Effect of Six-Wheel Vehicle on Crater Deflection Data

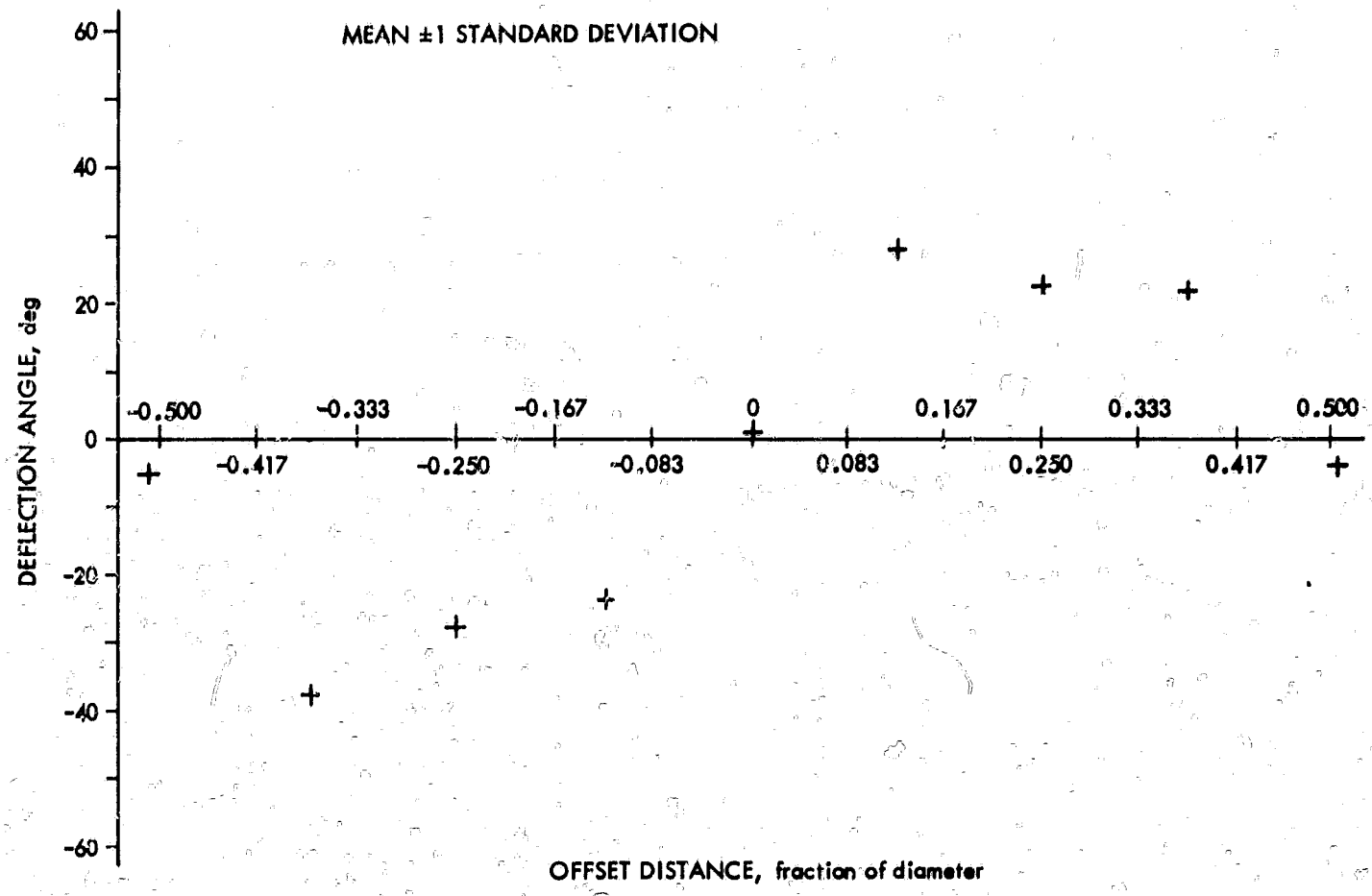

Figure 21. Crater Deflection Data, 47-ft Diameter, d/D Ratio 1:4.3

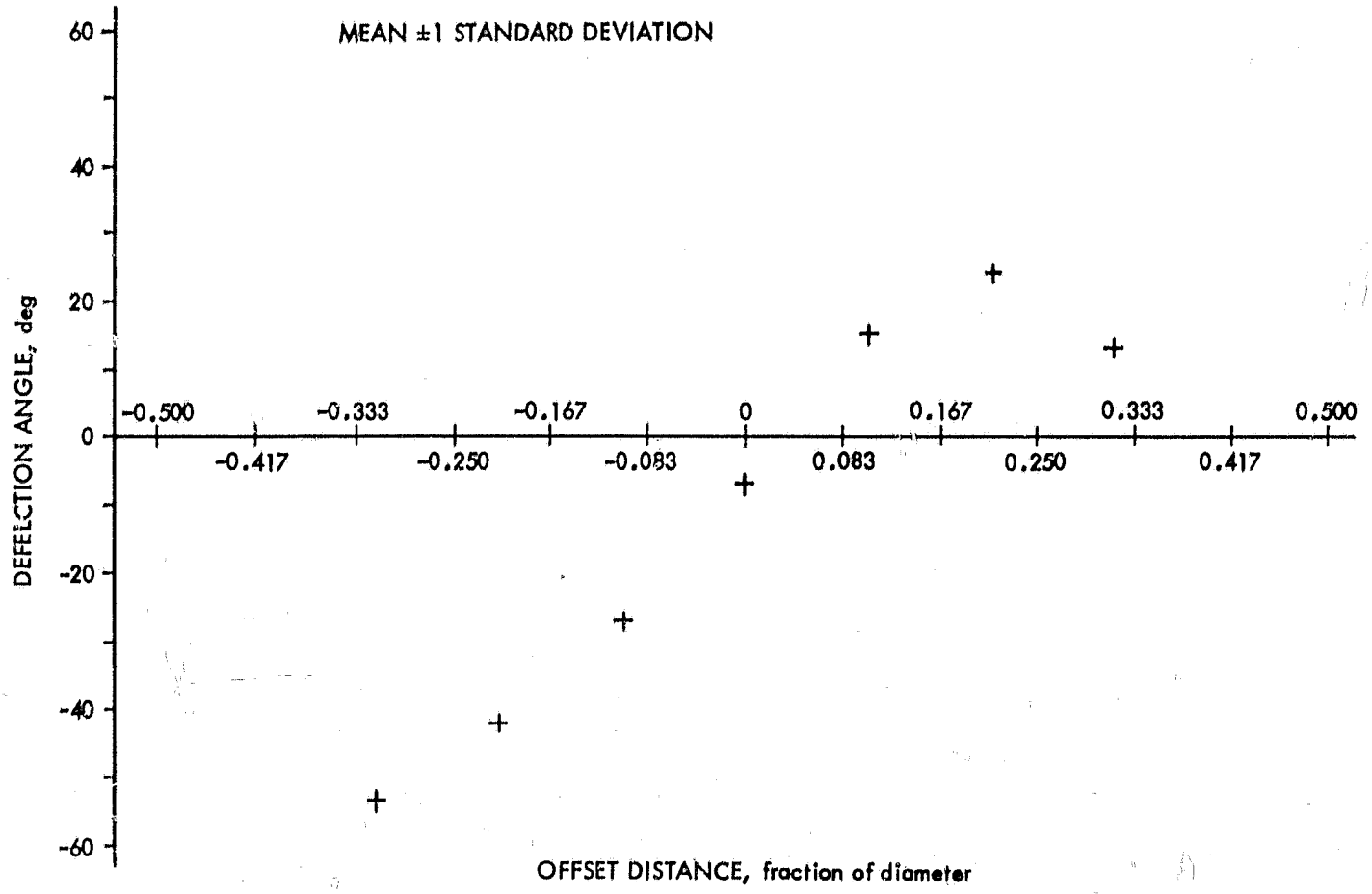

Figure 22. Crater Deflection Data, 57-ft Diameter, d/D Ratio 1:4.1

Table 1. Symmetry Indices for 36-in.-Diameter Craters

Depth to Diameter Ratio d/D	Symmetry Index				
	RMS_1	RMS_2	RMS_3	RMS_4	RMS_5
1:4	3.3	4.2	5.8	3.8	3.4
1:5	5.1	3.2	5.7	10.0	3.7
1:6	3.1	4.9	4.3	2.8	3.3
1:8	2.4	2.2	4.8	2.4	2.3
1:10	1.2	1.6	4.4	1.0	1.3
1:12	1.3	1.3	4.7	1.3	1.3
1:16	4.2	6.0	5.3	7.6	3.2
7-crater average	2.9	3.3	5.0	4.1	2.6

It is possible that systematic errors could have reduced the inherent symmetry of the results. Thus, certain corrections were applied to the 36-in.-diameter data, such as measuring the sample means from $\delta = \bar{\delta}(0)$ rather than $\delta = 0$. The symmetry index (see Table 1) is then given by

$$RMS_2 = \sqrt{\sum_a \left\{ \left[\bar{\delta}(a) - \bar{\delta}(0) \right] + \left[\bar{\delta}(-a) - \bar{\delta}(0) \right] \right\}}$$

In the search for systematic errors, a sample of 10 trial runs was made for each offset distance a on level ground. The crater-shaping tool was used to smooth the surface of sand after each run, and the offset distances were identical to those used in the 36-in.-diameter tests. (The vehicle had a slight tendency to pull to the right as indicated by a mean for all 130 trials of $\mu = 0.6$ deg. Standard deviation for 130 level-ground trials is $\delta = 1.0$ deg.) The sample means δ_o for these level-ground data (Figure 23) were used to correct the 36-in.-diameter data set. The symmetry index (see Table 1) for this set is

$$RMS_3 = \sqrt{\sum_a \left\{ \left[\bar{\delta}(a) - \bar{\delta}_o(a) \right] + \left[\bar{\delta}(-a) - \bar{\delta}_o(-a) \right] \right\}}$$

In an attempt to combine the aforementioned corrections, two additional corrections were applied to the 36-in.-diameter data set. Both take the first corrections $\delta(0)$, and modify it, first by the ratio of $\delta(a)$ to $\delta(0)$, and then by the reciprocal of that ratio. The combination corrections are then

$$\bar{\delta}(0) \cdot \bar{\delta}_o(a)/\bar{\delta}_o(0) \quad \text{and} \quad \bar{\delta}(0) \cdot \bar{\delta}_o(0)/\bar{\delta}_o(a)$$

respectively, and the symmetry indices computed for them are RMS_4 and RMS_5 (see Table 1).

An examination of Table 1 shows that the uncorrected data set has the lowest symmetry index RMS_1 in two of the seven craters. The RMS_5 set has a better average. However, considering the nature of the experiment and not having a clear association of the RMS_5 correction with systematic experimental bias, it is concluded that the uncorrected data are an adequate representation of the crater deflection phenomenon from the standpoint of symmetry.

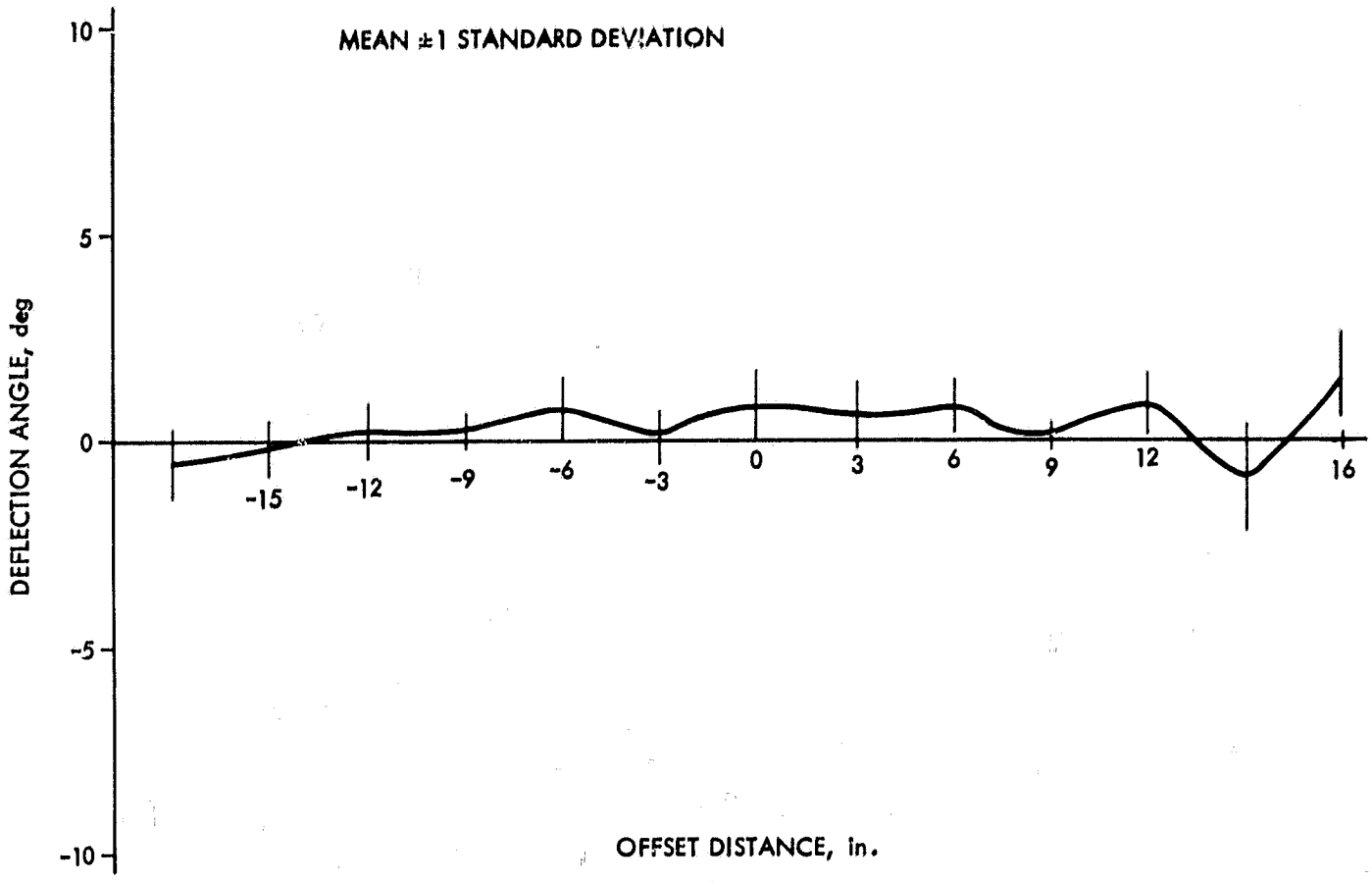

Figure 23. Crater Deflection Data, Sample Means for Level Ground

B. DEFLECTION REVERSALS

There is an observed tendency for the model vehicle to reverse the direction of deflection for $|a| > D/4$. This tendency was observed in Ref. 1 and was ascribed to wheel slippage as the vehicle climbed steep slopes. It was further noted in Ref. 1, and confirmed in these tests, that as wheels begin to slip, the stern of a vehicle swings so as to align its roll axis with the local slope gradient.

Figures 10 through 12 illustrate the phenomenon. The reversal is complete for d/D = 1:5 and d/D = 1:6 in the 36-in.-diameter craters. For approximately $0.33\,D < a < 0.45\,D$ the model vehicle has emerged from the crater in a direction slightly to the opposite side of the initial bearing from that expected without wheel slippage.

For shallower craters (see Figure 12) the reversal tendency is not discernible. For the steep, d/D = 1:4 crater (Figure 10), the suggestion of a reversal is seen in the pronounced "shoulder" in the deflection curve for the same range of "a" for which reversals occur at d/D = 1:5 and d/D = 1:6.

These results are supported by those for a 36-in. -diameter crater with d/D = 1:6 shown in Figure V-77 of Ref. 1. The model vehicle used in the referenced experiment was very similar to that used in these tests.

For the smaller craters, i.e., D = 30 in. and D = 24 in., the reversal tendency is slightly more obscure. The more shallow craters, (d/D = 1:8 through d/D = 1:12), again exhibit no clear evidence of a reversal due to slipping (Figures 14 through 16). The d/D = 1:6 curve for the 24-in. -diameter crater (Figure 15) is very similar to the same curve for the 36-in. -diameter crater (Figure 10).

However, the d/D = 1:4 series do not have the "shoulder" seen on the comparable curve for the 36-in. -diameter crater. For the 30-in. -diameter crater (Figure 13), there is a reversal tendency for d/D = 1:4 and d/D = 1:6, but the curves show little tendency to return close to $\delta = 0$ or to recross that axis at $D = \pm D/2$. An exception is the d/D = 1:6 curve at $D = -D/2$.

C. SAMPLE DISTRIBUTION

Because crater deflection is a stochastic process, the question arises as to the distribution of δ for a given combination of a, d/D, and D. Two sets of trial runs were made with 50 trials in each set for the purpose of assessing the statistical distribution of δ. The two 50-trial samples were made on 36-in. -diameter craters with d/D = 1:6, one at a = -9 in. and the second at a = +12 in.

Figures 24 and 25 indicate that the normal distribution with mean equal to the sample mean and variance equal to the sample variance may be a fair approximation. The statistic

$$D^2 = \sum_{i=1}^{k} (n_i - 50p_i)^2/50$$

was computed for each sample set, where k is the number of regions into which the sample space is divided, n_i is the number of samples in region i, and p_i is the theoretical probability of a sample within region i. Using maximum likelihood estimates of the theoretical mean and variance, one finds $D^2 = 6.95$ for the a = -9 in. sample set and $D^2 = 3.00$ for the a = +12 in. sample set. On the hypothesis that δ is normally distributed, a χ^2-test at the $\alpha = 0.05$ level of

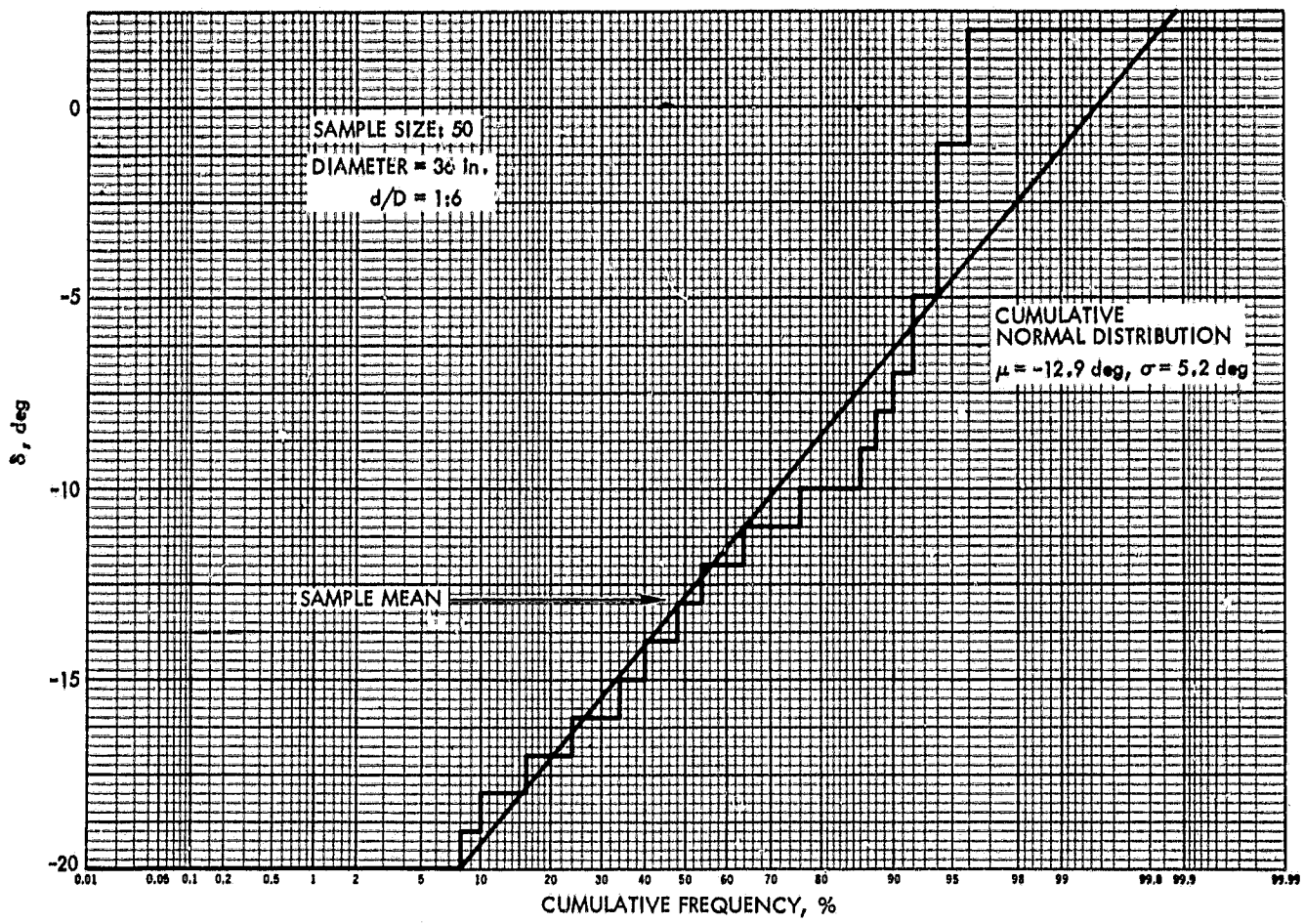

Figure 24. Cumulative Frequency Distribution, Offset Distance -9 in.

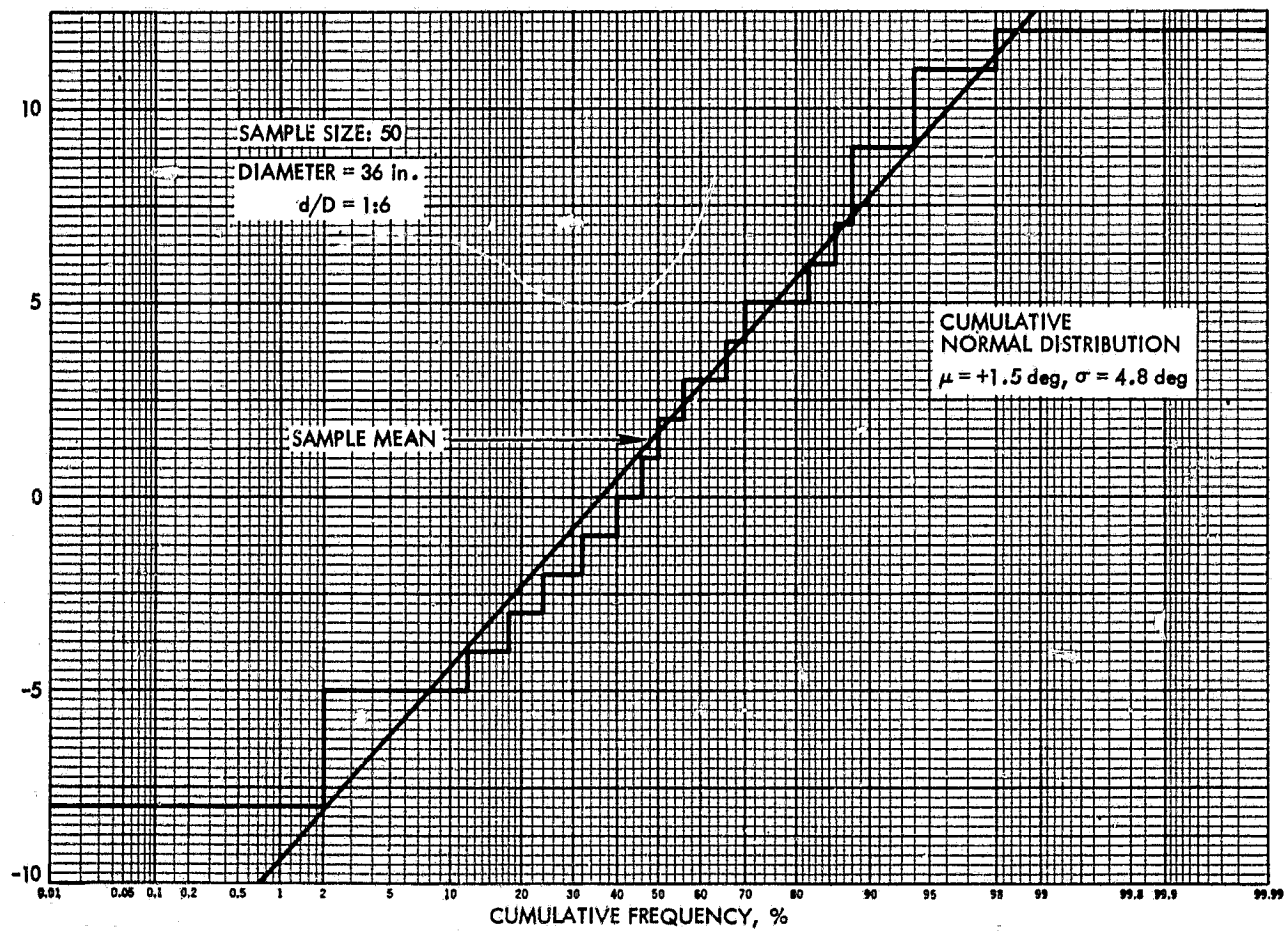

Figure 25. Cumulative Frequency Distribution, Offset Distance +12 in.

significance allows acceptance of that hypothesis (see Ref. 2, page 309). That is to say, it is specified that the probability of rejecting a normally distributed δ, when it is really true, is only 0.05. Under this condition the χ^2-test leads us to accept the hypothesis.

D. VARIATION IN CRATER GEOMETRY

Extensive variations in crater geometry were not made in these experiments. However, some inferences as to the effects of flat bottom craters can be drawn from Figure 17.

Both flat bottom craters show a reduction in the maximum excursion in δ when compared to the corresponding curve for D = 36 in. and d/D = 1:6 in Figure 11. The conical crater produced absolute deflections greater than 10 deg whereas only at a -D/2 for the flat bottom crater without raised rim is that deflection exceed in Figure 17.

Deflection reversals can be seen in both flat bottom craters. The reversals are more clearly developed with the raised rim crater. The crater without raised rim seems to localize the reversal about a = ±D/4.

E. SPECIAL TESTS

1. Tests of Model Vehicle with Varied Characteristics

A limited test was made in the variation of three model vehicle characteristics: (1) smaller wheels, (2) heavier vehicle, and (3) higher speed. A complete set of runs, i.e., 10 samples per offset, was made for each of these variations independently in a conical crater with D = 36-in. and d/D = 1:6 (Figures 18 and 19).

The smaller wheel was 2 3/4 in. in diameter, as compared with the 4 3/16 in.-diameter wheel of the same width. Fitted with the larger wheels, the model would travel 52% faster at the same number of wheel revolutions per minute.

Figure 18 shows distinct reversals, very similar to the comparable curve for large wheels in Figure 11. The amplitudes, or maximum excursions, of the two curves are also very similar if compensation is made for an apparent bias in the small wheel curve toward positive δ. The similarities in deflection curves imply that the smaller wheel did not result in significantly greater slipping.

The high-speed runs were 38% faster on the average, as measured in level-ground time trails, than the nominal-speed runs. Evidence for reversal is slight and maximum excursion in δ is about 10 deg. It seems that δ may be an increasing function of the time during which a vehicle is in the crater, assuming no steering and no stops.

Considering the small-wheels runs as low-speed runs, one can regard a wider speed range covered in these experiments. In the order low, standard, and high speed, the level-ground speeds were 0.38, 0.58 and 0.80 ft/sec, respectively. These observations would imply that there is a threshold speed between the second and third speeds at which the deflection curve begins to flatten and reversals are eliminated.

However, another conclusion supported by the limited evidence is that large wheels at a lower number of revolutions per minute would have produced larger reversals and larger amplitudes in δ. This would be consistent with a more gradual variation in the deflection effects caused by speed.

It is felt that the threshold explanation is more likely the correct one since slippage (and thereby deflection reversal) is more likely for the smaller wheel case than the larger. Lower footprint pressures of large wheels reduce slippage.

The results of increasing vehicle weight are rather inconclusive. A total of 110 g in ballast was added to the model vehicle producing a weight increase of 32%. The deflection curve in Figure 18 is not so symmetrical as similar curves. No conclusions are made as to the effects of increased weight.

2. Test of Six-Wheel Model Vehicle

A test series using a model with six small powered wheels was performed on a conical crater with 30-in.-diameter and d/D = 1:6. The smaller crater was selected for this special set of runs to provide space between the crater and edge of the sandbox for the longer vehicle.

The deflection curve in Figure 20 has some interesting characteristics and should be compared with the curve for a four-wheel vehicle in Figure 13 and with the small-wheel curve in Figure 18. The six-wheel data are quite symmetrical, suggesting that addition of the powered trailer to the four-wheel bus did not introduce a detectable bias in the deflection δ.

The maximum $\bar{\delta}$ of the six-wheel curve is about twice that of the four-wheel curve in Figure 13. Furthermore, this maximum deflection occurs in a range of offset distance a in which deflections are reversed. On the other hand, typical behavior of the four-wheel vehicle in all conical craters was that the maximum $\bar{\delta}$ is in the normal direction, i.e., positive δ for positive a and vice versa.

Comparison of the six-wheel data with the small-wheel data in Figure 18 shows them to be very similar. This suggests that wheel size is more responsible for the results in Figure 20 than the number of wheels. Further testing, for constant wheel sizes, would be necessary to determine whether deflections of a six-wheel vehicle are qualitatively different.

F. FULL-SCALE TEST RESULTS

Tests with the Explorer vehicle near Flagstaff, Ariz. intended to confirm observations of the model tests. Symmetry of δ about a = 0 is apparent in both the 47- and 57-ft-diameter craters (Figures 21 and 22).

Symmetry about $\delta = 0$ is not so apparent, particularly in the 57-ft-diameter crater. However, the distinct bias toward negative deflection in Figure 22 can be explained by a slow leak in Explorer's right front tire. This produced an increasing tendency for the vehicle to pull to the right. A level-ground test after the crater runs revealed a 9-deg deflection to the right in the first 100 ft and an additional 6-deg deflection to the right in the second 100 ft.

The 57-ft-diameter crater, even though it has one less data point, makes the best comparison with model results. Its 5.7:1 diameter-to-wheelbase ratio is close to the 5.5:1 ratio for the model 24-in. crater.

This comparison is made in Figure 26 by "folding" both the full-scale and model test results. For the full-scale data, $\pm[\delta(a)-\delta(-a)]/2$ is plotted with appropriate signs. New sample means are computed in a similar manner for the 24-in.-diameter and d/D = 1:4 data. The new sample size is 20, for which new sample variances are computed as well. The sample means plus and minus one standard deviation are plotted and connected by a curve to imply trends.

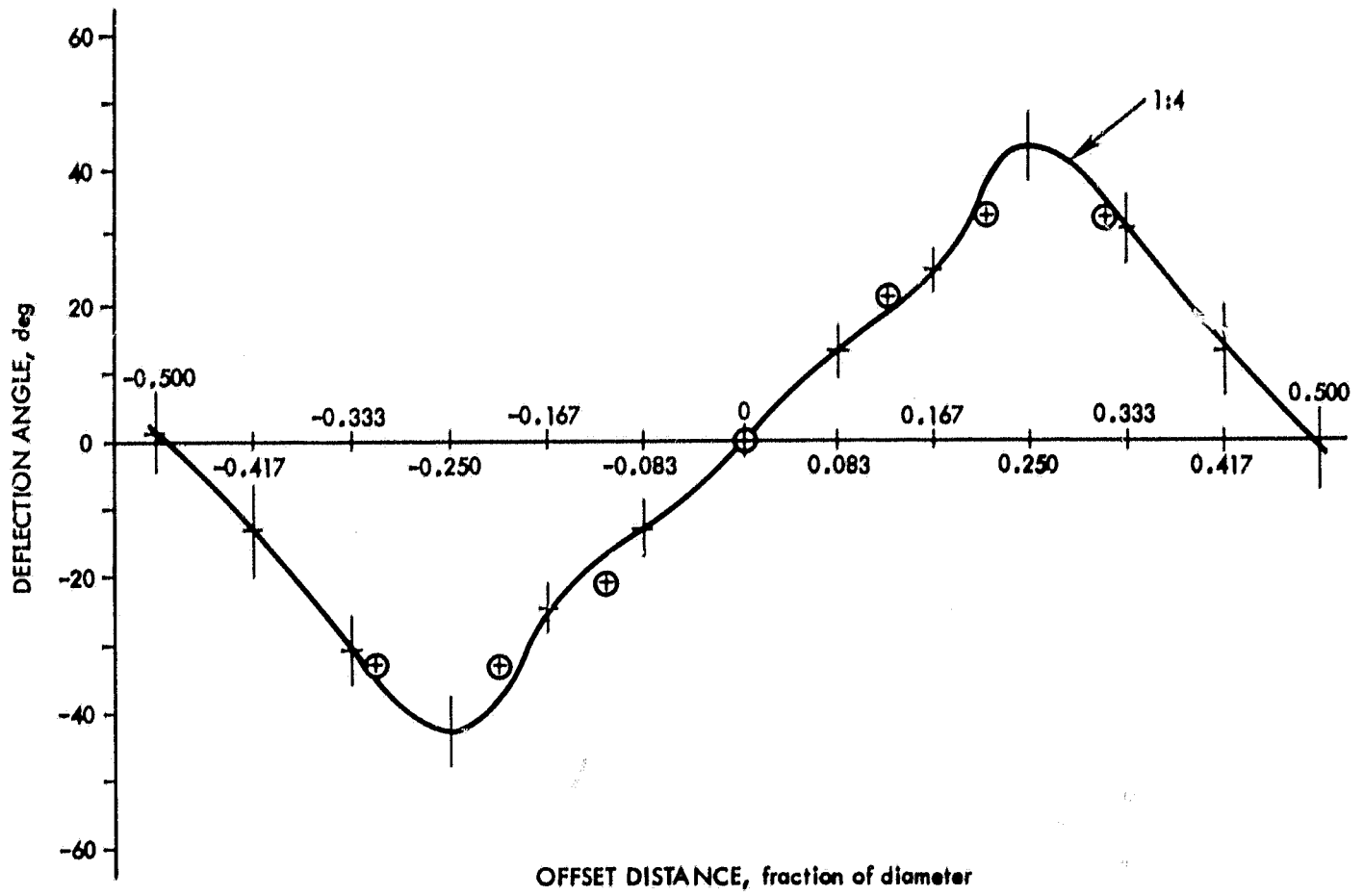

Figure 26. Comparison of Full-Scale and Model Test Data

The "folding" computation forces symmetry about the a = 0 and δ = 0 axes. Figure 26 clearly indicates a close correlation between the full-scale and model results, if one accepts the operations performed on the data. Therefore, the model tests appear to be a fair simulation of the crater deflection phenomenon. Close correlation at this one point helps lend credence to model test results in other shapes and sizes of craters.

REFERENCES

1. Burke, J. D., et al, "A Study of Lunar Traverse Mission," JPL Document 760-26, 16 September 1968.

2. Meyer, Paul L., "Introductory Probability and Statistical Applications," Addison-Wesley Publishing Company, Inc., 1965.

NASA — JPL — Coml., L.A., Calif.